Journal of Experimental Botany, Vol. 73, No. 11 pp. 3651–3670, 2022
https://doi.org/10.1093/jxb/erac057 Advance Access Publication 21 February 2022

RESEARCH PAPER

Infection by *Moniliophthora perniciosa* reprograms tomato Micro-Tom physiology, establishes a sink, and increases secondary cell wall synthesis

Daniele Paschoal[1,2], Juliana L. Costa[1], Eder M. da Silva[1], Fábia B. da Silva[2], Diogo Capelin[2], Vitor Ometto[1], Juliana A. Aricetti[3], Gabriel G. Carvalho[4], Rodrigo F. Pimpinato[1], Ricardo F. de Oliveira[2], Esther Carrera[5], Isabel López-Díaz[5], Mônica L. Rossi[1], Valdemar Tornisielo[1], Camila Caldana[6], Diego M. Riano-Pachon[1], Igor Cesarino[4], Paulo J.P.L. Teixeira[2], and Antonio Figueira[1,*]

[1] Centro de Energia Nuclear na Agricultura, Universidade de São Paulo, Piracicaba, SP, 13400-970, Brazil
[2] Escola Superior de Agricultura "Luiz de Queiroz", Universidade de São Paulo, Piracicaba, SP, 13418-900, Brazil
[3] Laboratório Nacional de Biorrenováveis, Centro Nacional de Pesquisa em Energia e Materiais, Campinas, SP, 13083-100, Brazil
[4] Instituto de Biociências, Universidade de São Paulo, São Paulo, SP, 05508-090, Brazil
[5] Universitat Politècnica de València (UPV), Consejo Superior de Investigaciones Científicas (CSIC), Valencia, Spain
[6] Max Planck Institute for Molecular Plant Physiology, 14476 Potsdam-Golm, Germany

* Correspondence: figueira@cena.usp.br

Received 26 August 2021; Editorial decision 9 February 2022; Accepted 15 February 2022

Editor: Yves Gibon, INRAE-Bordeaux, France

Abstract

Witches' broom disease of cacao is caused by the pathogenic fungus *Moniliophthora perniciosa*. By using tomato (*Solanum lycopersicum*) cultivar Micro-Tom (MT) as a model system, we investigated the physiological and metabolic consequences of *M. perniciosa* infection to determine whether symptoms result from sink establishment during infection. Infection of MT by *M. perniciosa* caused reductions in root biomass and fruit yield, a decrease in leaf gas exchange, and down-regulation of photosynthesis-related genes. The total leaf area and water potential decreased, while ABA levels, water conductance/conductivity, and ABA-related gene expression increased. Genes related to sugar metabolism and those involved in secondary cell wall deposition were up-regulated upon infection, and the concentrations of sugars, fumarate, and amino acids increased. ^{14}C-glucose was mobilized towards infected MT stems, but not in inoculated stems of the MT line overexpressing *CYTOKININ OXIDASE-2* (*35S::AtCKX2*), suggesting a role for cytokinin in establishing a sugar sink. The up-regulation of genes involved in cell wall deposition and phenylpropanoid metabolism in infected MT, but not in *35S::AtCKX2* plants, suggests establishment of a cytokinin-mediated sink that promotes tissue overgrowth with an increase in lignin. Possibly, *M. perniciosa* could benefit from the accumulation of secondary cell walls during its saprotrophic phase of infection.

Keywords: Cacao, cytokinin, lignin, saprotrophic, sugar, *Theobroma cacao*, witches' broom disease.

Introduction

Pathogenic fungi cause significant losses to crop production worldwide (Davies *et al.*, 2021). Fungal pathogens have distinct feeding strategies and can be categorized according to their lifestyle (Horbach *et al.*, 2011). Biotrophs require living tissues to grow and complete their life cycle, while necrotrophs kill host cells to thrive on dead tissue. Hemibiotrophs typically exhibit an initial short biotrophic stage before switching to a necrotrophic phase (Fernandez *et al.*, 2014). Saprotrophs feed on dead organic matter or decaying tissues (Smith *et al.*, 2017).

Infection by biotrophs or hemibiotrophs may directly impact the primary metabolism of hosts by diversion in the plant from growth to defence or by diversion of metabolites to the pathogen itself, in either case affecting relevant processes of plant development (Rojas *et al.*, 2014). To fulfil the energy demand for plant defence, some pathways associated with carbohydrate metabolism, such as glycolysis and the tricarboxylic acid cycle (TCA), are frequently induced in infected hosts (Berger *et al.*, 2007; Veillet *et al.*, 2017). A common consequence of fungal infection is the remobilization of photosynthates and other nutrients by inducing a strong sink at the infection site (Schultz *et al.*, 2013; Sosso *et al.*, 2019; Fernie *et al.*, 2020), usually by up-regulating genes such as *SUGAR TRANSPORTER PROTEINS* (*STPs*), sugar facilitators from the *SUGAR WILL EVENTUALLY BE EXPORTED TRANSPORTER* family (*SWEETs*), *SUCROSE TRANSPORTERs* (*SUTs*), and *CELL-WALL INVERTASEs* (*CWIVs*) (Pommerrenig *et al.*, 2020). Cytokinins are known to induce the establishment of sink tissues, commonly through the induction of *CWIVs*, *STPs* (Tauzin and Giardina, 2014; Albrecht and Argueso, 2017), and amino acid transporters [e.g. amino acid permeases (AAP), lysine and histidine transporters (LHT), and cationic amino acid transporters (CAT)], and promote the accumulation of hexoses and amino acids (Berger *et al.*, 2007; Veillet *et al.*, 2016; McIntyre *et al.*, 2021). The increased availability of hexoses during pathogen infection may cause the down-regulation of genes related to photosynthesis (Berger *et al.*, 2007), reducing the photosynthetic rate (Rojas *et al.*, 2014; Matei *et al.*, 2018).

Cytokinins are plant hormones that regulate several mechanisms of plant growth and development, and may act as positive regulators of pathogen virulence (Chanclud and Morel, 2016). Usually, the involvement of cytokinins in plant–pathogen interactions is associated with the establishment of a strong sink at the site of infection, mostly related to their role in cell division (McIntyre *et al.*, 2021). Infection of hosts by the cytokinin-producing pathogens *Rhodococcus fascians* (the causal agent of leafy gall disease) and *Plasmodiophora brassicae* (the causal agent of the clubroot disease of Brassicaceae) was shown to increase the expression of sugar-related genes, transforming the infection site into a strong sink (Pertry *et al.*, 2009; Dhandapani *et al.*, 2017; Walerowski *et al.*, 2018; Zhang *et al.*, 2019*a*). The fungal maize pathogen *Ustilago maydis* produces cytokinins and induces sink formation through the expression of host *STPs* and *SWEETs*, with the consequent accumulation of hexoses for pathogen feeding (Bruce *et al.*, 2011; Sosso *et al.*, 2019). The rice pathogen *Magnaporthe oryzae* was also reported to produce cytokinins and induce the accumulation of nutrients at the site of infection (Chanclud *et al.*, 2016).

Abscisic acid (ABA) is another plant hormone that, despite its recognized role in water-stress responses (Kuromori *et al.*, 2018), was shown to regulate the increase in sink strength during host infection by some pathogens (Hayes *et al.*, 2010; Morrison *et al.*, 2017; Huai *et al.*, 2019). Infection of grapevine by *Erysiphe necator* or *Plasmopora viticola* increased the expression of *CWIV*, *VvcwINV*, and the hexose transporter *VvHT5*, enhancing sink strength through ABA regulation (Hayes *et al.*, 2010). Similarly, infection of wheat by *Puccinia striiformis* f. sp. *tritici* stimulates ABA biosynthesis, leading to increased expression of the hexose transporter gene *TaSTP6*, while promoting sugar supply and pathogen infection (Huai *et al.*, 2019).

The basidiomycete *Moniliophthora perniciosa* causes witches' broom disease (WBD) of cacao (*Theobroma cacao*). WBD is restricted to South American and Caribbean cacao-producing countries, where it severely impacts cacao production (Artero *et al.*, 2017). In cacao, germinating *M. perniciosa* basidiospores penetrate only active meristematic tissues. The monokaryotic hyphae grow slowly, colonizing the apoplast at low density during the biotrophic phase of infection (Sena *et al.*, 2014), which is unusually long (up to 90 d) for a hemibiotroph (Teixeira *et al.*, 2014). Biotrophic infection promotes remarkable symptoms, including the loss of apical dominance and the induction of hypertrophic growth of axillary shoots (Purdy and Schimdt, 1996). Eventually, the hyphae of the pathogen form clamp connections and become dikaryotic, and the cacao tissues become necrotic due to an undetermined cause (Sena *et al.*, 2014). *Moniliophthora perniciosa* belongs to the Marasmiaceae, which contains mostly saprotrophic litter- and wood-decomposing species (Lisboa *et al.*, 2020), but *M. perniciosa* has been considered a hemibiotroph. A novel classification based on the genome content of genes encoding carbohydrate-active enzymes (CAZymes) predicted *M. perniciosa* to be a saprotroph (Hane *et al.*, 2020).

Biochemical and transcriptional changes related to cacao shoot primary metabolism during infection with *M. perniciosa* have been described (Scarpari *et al.*, 2005; Barau *et al.*, 2014; Teixeira *et al.*, 2014). An analysis of infected shoots indicated an increase in glucose, fructose, sucrose, purine alkaloids, and asparagine (Scarpari *et al.*, 2005). Transcriptional profiling of the biotrophic stage of infection revealed metabolic reprogramming (Teixeira *et al.*, 2014), resulting in increased activity of a cell-wall invertase in the apoplast, reduced levels of sucrose, and increased levels of glucose and fructose, suggesting the development of a sugar sink in infected cacao shoots (Barau *et al.*, 2014) and the activation of premature senescence (Teixeira *et al.*, 2014).

Cacao, as a perennial tree species, is a challenging non-model biological system. *Moniliophthora perniciosa* can infect diverse hosts, including several Solanaceae species, inducing shoot symptoms similar to those observed in infected cacao (Lisboa *et al.*, 2020). The C-biotype of *M. perniciosa* is pathogenic only to *Theobroma* and *Herrania* species, whereas the S-biotype infects mostly wild Solanaceae species (Pierre *et al.*, 2017). The tomato (*Solanum lycopersicum*) cultivar Micro-Tom (MT) is susceptible to the S-biotype upon inoculation, and it has been used as a model to investigate pathogenesis (Deganello *et al.*, 2014). The short life cycle (90 d) and small size of MT plants are highly attractive characteristics for exploring the molecular and physiological aspects of interaction with pathogens (Carvalho *et al.*, 2011).

Previously, we have demonstrated that the S-biotype of *M. perniciosa* produces cytokinins *in vitro* and interferes with the cytokinin balance in infected tomato plants (Costa *et al.*, 2021). We inoculated an MT transgenic line that overexpresses the Arabidopsis *CYTOKININ OXIDASE-2* gene (*35S::AtCKX2*) (Pino *et al.*, 2010). We recently showed that this line had lower levels of cytokinins, and we observed a lower incidence of infection and reduced symptoms compared with infected wild-type MT (Costa *et al.*, 2021). As expected (Werner *et al.*, 2003), the transgenic plants showed retarded shoot development and enhanced root growth. RNA-seq analysis of infected MT plants revealed the up-regulation of a set of cytokinin-related marker genes in comparison to non-inoculated control plants (Costa *et al.*, 2021). MT plants treated with benzyladenine (BA) developed similar infection symptoms, while *M. perniciosa*-infected plants treated with cytokinin-receptor inhibitors LGR-991 and PI55 showed less pronounced symptoms. We hypothesized that the change in the cytokinin balance may be associated with the manipulation of sink establishment in favour of fungal infection. In cacao, yield losses are thought to derive mostly from pod rot, but they might involve the debilitation of plants via the remobilization of energy resources to infected tissues during the biotrophic phase of infection (Teixeira *et al.*, 2014). Thus, the physiological reasoning behind losses in cacao yield is not yet fully explained.

Here, we characterized the physiological and metabolic responses of tomato MT to *M. perniciosa* infection. We evaluated physiological parameters of symptomatic tissues of MT plants, and analysed genes involved in plant metabolism by RNA-seq analysis. Concentrations of ABA and the translocation of ^{14}C-glucose in infected MT and *35S::AtCKX2* plants were evaluated. The results point to the induction of a strong sink at the infected stem, along with the up-regulation of genes involved in cell wall deposition and phenylpropanoid metabolism, and the accumulation of lignin in MT stems, but not in the *35S::AtCKX2* line. It is possible that *M. perniciosa* could benefit from the accumulation of secondary cell walls (SCWs) during its saprotrophic phase of infection.

Materials and methods

Plant material

Tomato MT and an MT line overexpressing Arabidopsis *CYTOKININ OXIDASE-2* (*35SS::AtCKX2*) (Pino *et al.*, 2010) were used in the inoculation experiments. Plants were grown as described by Costa *et al.* (2021).

Inoculation experiments

Dry brooms from the Tiradentes isolate were obtained from *Solanum lycocarpum* naturally infected with *M. perniciosa*, basidiospores were collected from detached pilei, and MT plants were inoculated as reported by Costa *et al.* (2021). Symptoms of infection in the MT plants were evaluated at 5, 15, 25, and 35 days after inoculation (dai). Root and stem dry weight, main root length, and fruit number and dry weight were determined at 40 dai in a completely randomized design (n=10). Significant differences were determined by Student's t-test at P<0.05 using R software (R Core Team, 2020).

Detection of *M. perniciosa* in infected MT tissues by DNA amplification

Stem sections taken between the first and second leaves and roots of inoculated and non-inoculated MT plants were collected at 35 dai (n=3), frozen, ground in a cryogenic mill (CryoMill, Retsch, Haam, Germany), and used for DNA extraction (Doyle and Doyle, 1990). DNA from *in vitro*-grown *M. perniciosa* mycelia (Costa *et al.*, 2021) was used as a positive control. Primers specific for the *M. perniciosa RPL35* gene (MP14350, WBD Transcriptome Atlas; Teixeira *et al.*, 2014) (ACTTCGGGTGCAAAAGATTG and TGGTCCTTCTTCGTCTGCTT; Deganello *et al.*, 2014) and for the tomato actin *SlActin* gene (Solyc04g011500.2.1; GGTCCCTCTATTGTCCACAG and TGCATCTCTGGTCCAGTAGGA) were used in amplification reactions. Reactions were performed in a 12.5 µl total volume, containing 100 ng of DNA, 3.75 mM $MgCl_2$, 0.2 mM dNTPs, 0.5 µM of each primer, and 2.5 U *Taq* DNA polymerase in appropriate buffer. The amplification reactions were conducted with an initial denaturation step of 3 min at 95 °C, followed by 35 cycles of 30 s at 94 °C, 40 s at 60 °C, and 30 s at 72 °C, and a final step of 10 min at 72 °C. No DNA template control was included. Products were visualized by gel electrophoresis in 1.5% agarose gel.

Gas exchange analyses

Net assimilation of CO_2 (A, µmol m^{-2} s^{-1}), transpiration rate (E, mmol m^{-2} s^{-1}), stomatal conductance (g_s, mol H_2O m^{-2} s^{-1}), and intercellular CO_2 concentration (Ci, µmol m^{-2} s^{-1}) were determined using an infrared gas analyser (LI-6400XT, LI-COR, Lincoln, NE, USA) coupled with a fluorescence chamber (6400-40, LI-COR). The analyses were conducted at 25 °C, with photosynthetically active radiation at 800 µmol m^{-2} s^{-1}, atmospheric CO_2 concentration at ~400 µmol mol^{-1}, and relative humidity at ~60%. Gas exchange analysis was conducted on the second and third, symptomatic (chlorotic) or asymptomatic (non-chlorotic), leaves of infected MT plants at 25 dai and compared with equivalent leaves of non-inoculated MT plants in a completely randomized design (n=10). Significant differences were determined by Student's t-test at P<0.05 using R software.

Determination of leaf water potential and total leaf area

Leaf water potential (MPa) was estimated using a psychrometer (PSYPRO, Wescor, Logan, UT, USA) coupled to a C52 chamber. Leaf

discs from the second and third, symptomatic (chlorotic) or asymptomatic (non-chlorotic), leaves of infected MT plants at 35 dai were analysed and compared with equivalent leaves of non-inoculated MT plants. Total leaf area (cm^2) was determined using a LI-3100C leaf-area integrator (LI-COR). The experimental design was completely randomized (n=10). Significant differences were determined by Student's t-test at P<0.05 using R software.

Stem hydraulic conductance and conductivity analysis

Stem segments of infected plants were fractionated into symptomatic (thickened) or non-symptomatic (above the thickened region) portions and compared with equivalent segments from non-inoculated MTplants at 35 dai. The hydraulic conductance determines the amount of water translocated through a stem section over a period of time, while the hydraulic conductivity establishes the flow rate at a given pressure when water is translocated throughout the length of a stem segment (Nardini and Tyree, 1999; Atkinson *et al.*, 2003). Stem segments were connected to silicone tubing linked to a peristaltic pump. The base of the stem segment was submerged in water, and tension (0.03 MPa) was applied to the hydraulic system to promote suction of water through the segment. The tension draws the flow-through water from the stem segment to a dry cotton ball (Ehlert *et al.*, 2009). The volumetric rate (Jv, in $m^3\ s^{-1}$) of water translocated through the stem vascular system by the applied tension (T, in MPa) and the stem area (A, in m^2) is calculated by

$$J_v = \frac{P_u - P_s}{t \times \rho},$$

where Pu is the final weight of the cotton ball (kg), Ps is the initial weight of the cotton ball (kg), t is the time interval (s^{-1}), and ρ is the water density ($kg\ m^{-3}$). The stem hydraulic conductance (K_{stem} in $m^3\ MPa^{-1}\ s^{-1}$) is calculated by

$$K_{stem} = \frac{Jv}{T \times A}.$$

The stem hydraulic conductivity ($K_{h,}$ in $kg\ ms^{-1}\ MPa^{-1}$) (Pivovaroff *et al.*, 2014) is calculated by

$$K_h = \frac{F \times L}{\Delta p}$$

where F is the flow rate ($kg\ s^{-1}$), L is the stem segment length (cm), and Δp is the variation of tension applied (MPa). The experiment was completely randomized (n=9). Significant differences were determined by Student's t-test at $P < 0.05$ using R software.

RNA-seq analysis

RNA-seq reads were obtained from the NCBI Gene Expression Omnibus (GEO, https://www.ncbi.nlm.nih.gov/geo/) (#GSE153345) and reanalysed. The transcriptomic data were originally obtained from stem sections from between the first and second leaves collected at 5, 10, 20, and 30 dai (n=5 per time point) for MT, and at 30 dai for the *35S::AtCKX2* line (n=5) (Costa *et al.*, 2021). The read quality was evaluated using FastQC/0.11.8 (Andrews, 2010) and trimmed using the BBduk tool of the BBMap package (https://sourceforge.net/projects/bbmap/) and Trimmomatic (Bolger *et al.*, 2014). The cleaned reads were mapped against the tomato transcriptome ITAG3.1 and quantified using Salmon (Patro *et al.*, 2017). Read counts were retrieved using the R package tximport (https://bioconductor.org/packages/release/bioc/html/tximport.html), and data were converted into lengthScaledTPM (Soneson *et al.*, 2015). Differential gene expression was analysed as described by Costa *et al.* (2021). We used MapMan (Thimm *et al.*, 2004) to classify the differentially expressed genes (DEGs) into defined hierarchical categories (BINs). Heatmaps of expression profiles of significant DEGs were generated using the R package pheatmap (Kolde, 2018); clusters were obtained using the cuttree function (Montero *et al.*, 2014).

Quantification of ABA

Stems of inoculated MT and *35S::AtCKX2* plants were used to estimate ABA concentrations, as previously described (Costa *et al.*, 2021). Stem sections taken between the first and second leaves were collected at 5, 10, 20, and 30 dai (n=5 per time point) for MT, or at 30 dai (n=5) for the *35S::AtCKX2* line. ABA was extracted as described by Martínez-Bello *et al.* (2015) and analysed as described by Costa *et al.* (2021). Significant differences were determined by two-way ANOVA, followed by comparison of means by the Tukey test at P<0.05 using R software.

Analysis of primary metabolites

Stem sections taken between the first and second leaves of inoculated or non-inoculated MT, collected at 4, 10, and 20 dai, were ground in a cryogenic mill (n=5 per time point). Metabolites were extracted from 50 mg of samples using methyl-*tert*-butyl-ether (MTBE):methanol:water (3:1:1, v/v) (Giavalisco *et al.*, 2011). Samples were homogenized for 10 min at 4 °C, incubated for 10 min in a cooled sonicator, vortexed, and centrifuged at 13 000 *g* for 5 min at 4 °C. Then, 150 µl of the polar fraction was collected and dried. The dry extract was dissolved and derivatized in methylamine–HCl and *N*-methyl-*N*-trimethylsilyl fluoroacetamide (MSTF) for 90 min at 30 °C, and a standard mixture of retention-time indices was added and kept for 30 min at 37 °C (Roessner *et al.*, 2000). Volumes of 1 µl of the derivatized samples were analysed using a CombiPAL autosampler (Agilent Technologies, Waldbronn, Germany) coupled to an Agilent 7890A gas chromatograph (GC) and a Leco Pegasus HT time-of-flight mass spectrometer (TOF-MS) (LECO, St. Joseph, MI, USA). The chromatograms were exported from Leco ChromaTOF (v. 4.51.6.0) into cdf files to be processed in R software (R core Team, 2020). TargetSearch (Bioconductor) was used for peak detection and retention-time alignment (Cuadros-Inostroza *et al.*, 2009). For metabolite identification, the extracted mass spectra and retention times were queried against the Golm Metabolome Database reference library (http://gmd.mpimp-golm.mpg.de/). Metabolites were quantified by the intensity of peaks by quantitative mass. Normalization of metabolite intensity was achieved by dividing fresh weight and ion counts (Giavalisco *et al.*, 2011), and data were normalized by dividing each value by the average of all measures for one metabolite. Principal component analysis was conducted employing pcaMethods in Bioconductor (Stacklies *et al.*, 2007). The effects of treatment were assessed by ANOVA, followed by Tukey's test using R software. The heatmap was constructed with the R package 'pheatmap' version 1.0.12.

^{14}C-glucose mobilization assay

In the first experiment, MT or *35S::AtCKX2* plants, inoculated with *M. perniciosa* or non-inoculated, were treated with 10 µl of ^{14}C-glucose (312.583 Bq μl^{-1}) applied to the first leaf above the inoculation site at 4, 10, and 20 dai (n=6). The treated plants were kept at room temperature for 6 h and then separated into organs and weighed, and each organ was oxidized (Biological Oxidizer OX500, Harvey Instrument; Tappan, NY, USA). The resulting $^{14}CO_2$ was fixed in scintigraphy buffer, quantified by liquid scintigraphy spectrometry (Liquid Scintillation Analyser 1600 TR, Packard Canberra; Schwadorf, Austria), and expressed in specific

radioactivity (Bq mg^{-1}). In the second experiment, stock solutions of 1 M BA dissolved in DMSO were diluted in lanolin (1:49) heated to 55 °C (Roman *et al.*, 2016; Costa *et al.*, 2021). Volumes (12 µl in total) of 20 mM BA were applied to the shoot apices and axillary buds of MT plants (n=15) and again 10 d after the first application; control plants received DMSO:lanolin at 1:49 (n=6). The remobilization of ^{14}C-glucose was estimated in MT plants treated with BA or untreated controls, collected at 5, 10, and 20 days after application (daa) of BA (n=6). Significant differences were determined by Student's t-test at P<0.05 using R software.

Lignin quantification

Stem sections taken between the first and second leaves of inoculated or non-inoculated MT plants were collected at 30 dai, frozen, ground in a cryomill, and freeze-dried. Samples were used to estimate total lignin (% cell wall) (n=9). Samples were subjected to sequential extraction to prepare the cell wall residue. The extractions were performed for 30 min each at near-boiling temperature in water (98 °C), ethanol (76 °C), chloroform (59 °C), and acetone (54 °C), and the resulting cell wall residue was dried at 60 °C overnight. Lignin quantification was performed using the acetyl bromide method (Fukushima and Kerley, 2011). Significant differences were determined by Student's t-test at P<0.05 using R software.

Lignin staining of MT stem cross-sections

Stems from infected or non-inoculated MT plants were collected at 30 dai (n=5). Fresh stem fragments taken between the first and second leaves were sectioned using a microtome (SM200R, Leica, Heidelberg, Germany). The sections were specifically stained for lignin with phloroglucinol–HCl (Jensen, 1962). Slides were covered with glycerol and immediately observed under a Leica EZ4E stereomicroscope (Leica Biosystems, Nussloch, Germany) with apochromatic optics (S8AP0; Leica).

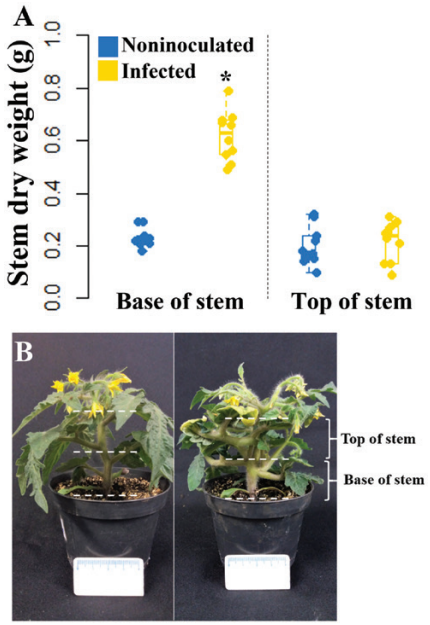

Fig. 1. Quantification of stem swelling in tomato Micro-Tom (MT) plants infected with the S-biotype of *Moniliophthora perniciosa*. (A) Dry weight of 3 cm stem segments around the first leaf (base of stem) from non-inoculated or infected symptomatic plants, and from stem segments above the symptomatic region from non-inoculated or infected symptomatic plants, at 35 dai (n=10). In each boxplot, the middle line represents the median value, the upper and lower bars correspond to the first and third quartiles, respectively, and the whiskers represent 1.5 times the interquartile range. Statistically significant differences were determined by the t-test and are indicated with asterisks (*P<0.05). (B) Indication of the sampled stem segments of non-inoculated (left) and infected (right) MT plants. Scale bar=4 cm.

Results

Infection with M. perniciosa *increased the weight of symptomatic stems and reduced fruit yield*

Using the MT model system, we previously described symptoms such as stem swelling, a reduction in root biomass, and an increase in fruit locule number in response to infection with *M. perniciosa* (Costa *et al.*, 2021). Here, we inoculated MT plants and observed, in addition to the typical symptoms (Supplementary Fig. S1A, B, F, G, K, L), leaves near the site of infection that were wrinkled and chlorotic at the edges, and thickened petioles, leaf veins, and floral peduncles at 35 dai (Supplementary Fig. S1C–E, H–J).

The infected swollen stem segments showed a significant increase in dry weight compared with equivalent segments of non-inoculated plants (Fig. 1A, B), proportional to the increase in stem diameter (Costa *et al.*, 2021). As a control, we determined the dry weight of non-symptomatic stem segments above the symptomatic sections and compared it with the dry weight of equivalent stem segments of non-inoculated plants; no significant differences were observed (Fig. 1A, B). The severity of swelling symptoms progressed over time, and the symptomatic stem remained green, with few necrotic spots, as late as 90 dai (Supplementary Fig. S2).

Infection resulted in a significant decrease in the total number of fruits produced per plant (Fig. 2A) and in total fruit dry weight per plant (Fig. 2B) at 35 dai. We observed a reduced number of flowers after anthesis per plant at 20 dai (Supplementary Fig. S3A), along with the repression of DEGs related to flowering (e.g. *CONSTANS*, *AGAMOUS*, *APETALA*) at the infection site at 20 dai and 30 dai, as determined by RNA-seq (Supplementary Fig. S3B). The root system of infected plants showed impaired growth, with reduced total root dry weight at 35 dai (Fig. 2C), but no difference in the main root length (Fig. 2D).

To determine the systemic presence of the pathogen in infected tissues, we amplified fragments of a *M. perniciosa*-specific gene (*MpRPL35*) and a host gene as a normalizer (*SlActin*) using DNA from stems and roots of infected or non-inoculated MT plants. *MpRPL35* was detected only in symptomatic stem samples from infected plants (Supplementary Fig. S4A), and no amplification occurred in samples from roots or in samples from non-inoculated plants (Supplementary Fig. S4B).

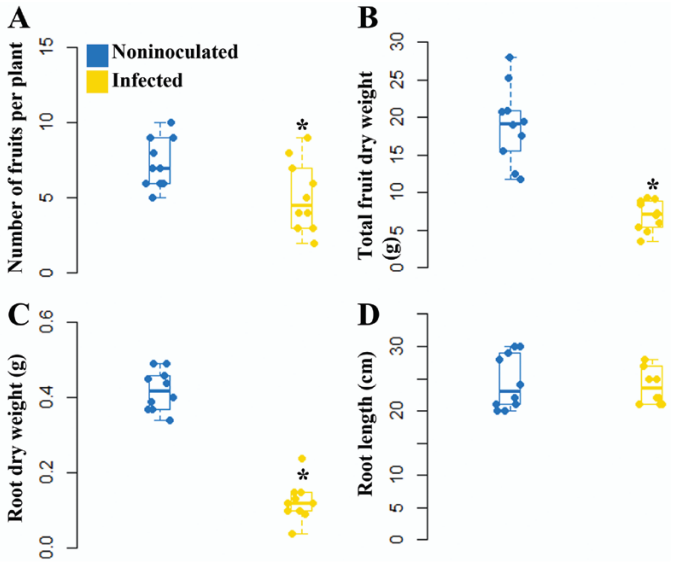

Fig. 2. Effect of infection of tomato Micro-Tom plants by the S-biotype of *Moniliophthora perniciosa* on fruit yield and root development. (A) Total number of fruits per plant, (B) total fruit dry weight per plant, (C) root dry weight, and (D) root length of non-inoculated or infected MT plants at 35 dai (n=10). In each boxplot, the middle line represents the median value, the upper and lower bars correspond to the first and third quartiles, respectively, and the whiskers represent 1.5 times the interquartile range. Statistically significant differences between infected and non-inoculated control plants were determined by the t-test and are indicated with asterisks (*P<0.05).

Infection reduces leaf net photosynthesis and stomatal conductance while increasing water conductance and conductivity in infected stems

MT plants infected with *M. perniciosa* showed a significant decrease in net photosynthesis (A) in symptomatic (chlorotic and wrinkled) leaves and in adjacent non-symptomatic (non-chlorotic) leaves compared with leaves at the same developmental stage and position in non-inoculated plants (Fig. 3A). A significant decrease in g_s (Fig. 3B) and E (Fig. 3C) was detected only in symptomatic leaves. In contrast, Ci was increased in symptomatic leaves compared with leaves of non-inoculated plants (Fig. 3D).

Using the RNA-seq data (NCBI GEO #GSE153345), we analysed the expression profile of DEGs related to photosynthesis in symptomatic tissues at 20 dai and 30 dai by employing hierarchical clustering (Fig. 3E; Supplementary Fig. S5). In infected stems, we detected decreased expression of DEGs related to the photosynthetic apparatus, electron carriers, and the Calvin cycle, including those that encode chlorophyll *a*/*b*-binding proteins, subunits of the photosystem reaction centre, ferredoxin, the small subunit of ribulose bisphosphate carboxylase, glyceraldehyde-3-phosphate dehydrogenase, and fructose-1,6-bisphosphatase, compared with expression in the stems of non-inoculated plants (Fig. 3E).

To investigate the impact of the reduced root system of infected MT plants, presuming that this imposed a constraint on water uptake, we estimated the leaf water potential. Water potential decreased in both symptomatic and non-symptomatic leaves of infected plants (Fig. 4A), which might contribute to the observed reduction in g_s (Fig. 3B). Total leaf area per plant was significantly reduced in infected plants (Fig. 4B). We also observed the up-regulation of some DEGs related to ABA signalling, including those that encode ABA-responsive protein, receptors (PYR/PYL/RCAR), S-type channel anion proteins, and a plasma membrane intrinsic protein, whose best hit in Arabidopsis was the aquaporin *PIP2;1* (Fig. 4C). ABA concentrations decreased in non-inoculated MT stems at 20 dai and 30 dai, while infection impaired this reduction, with more ABA being detected in infected MT stems (Fig. 4D). We also quantified ABA in inoculated *35S::AtCKX2* plants. Non-inoculated *35S::AtCKX2* plants showed a higher ABA concentration than non-inoculated MT plants at 30 dai, while inoculation of *35S::AtCKX2* plants did not result in increased ABA concentrations (Fig. 4D).

We investigated whether water conductance and conductivity were affected in infected symptomatic stems, which are associated with hypertrophic growth of the vascular tissue (Marelli *et al.*, 2009; Costa *et al.*, 2021). Compared with the equivalent segment in non-inoculated plants, hydraulic conductance (Fig. 5A, C) and conductivity rates (Fig. 5B, C) were higher in the infected symptomatic stem. Conversely, the non-symptomatic region of the stem, above the symptomatic region, had hydraulic conductance (Fig. 5A, C) and conductivity rates (Fig. 5B, C) similar to those of the stem in non-inoculated plants.

Transcriptional reprogramming of infected stems suggests growth and induction of a nutrient sink

We analysed the RNA-seq data of infected MT stems and non-inoculated controls at 5, 10, and 20 dai. Transcriptional analysis pointed to the metabolic reprogramming of infected stems over time, especially at 20 dai, when symptoms were evident (Supplementary Table S1). Genes associated with starch anabolism and catabolism were down-regulated, including those encoding β-amylases, ADP-glucose pyrophosphorylase small subunits, granule-bound starch synthase, callose synthase, and cytosolic malate dehydrogenase (Fig. 6A). Conversely, genes encoding proteins related to sugar sensing and signalling [e.g. Trehalose-6-Phosphate Synthase 1 (TPS1), Trehalose 6-Phosphate Phosphatase (TPP)], a phosphotransferase orthologue of Arabidopsis hexokinase-3 and -4, H^+/monosaccharide transporters (e.g. STP1 and STP12), and polyol and tonoplast monosaccharide transporters (Fig. 6A) were induced. Notably, we found overexpression of a cell-wall invertase (*INVERTASE 6*) required for sucrose breakdown in the apoplast (Fig. 6A). Regarding amino acid metabolism, genes encoding an arogenate dehydrogenase, amino acid and nitrate transporters, glutamate synthase, and proline dehydrogenase were up-regulated at 20 dai (Fig. 6B).

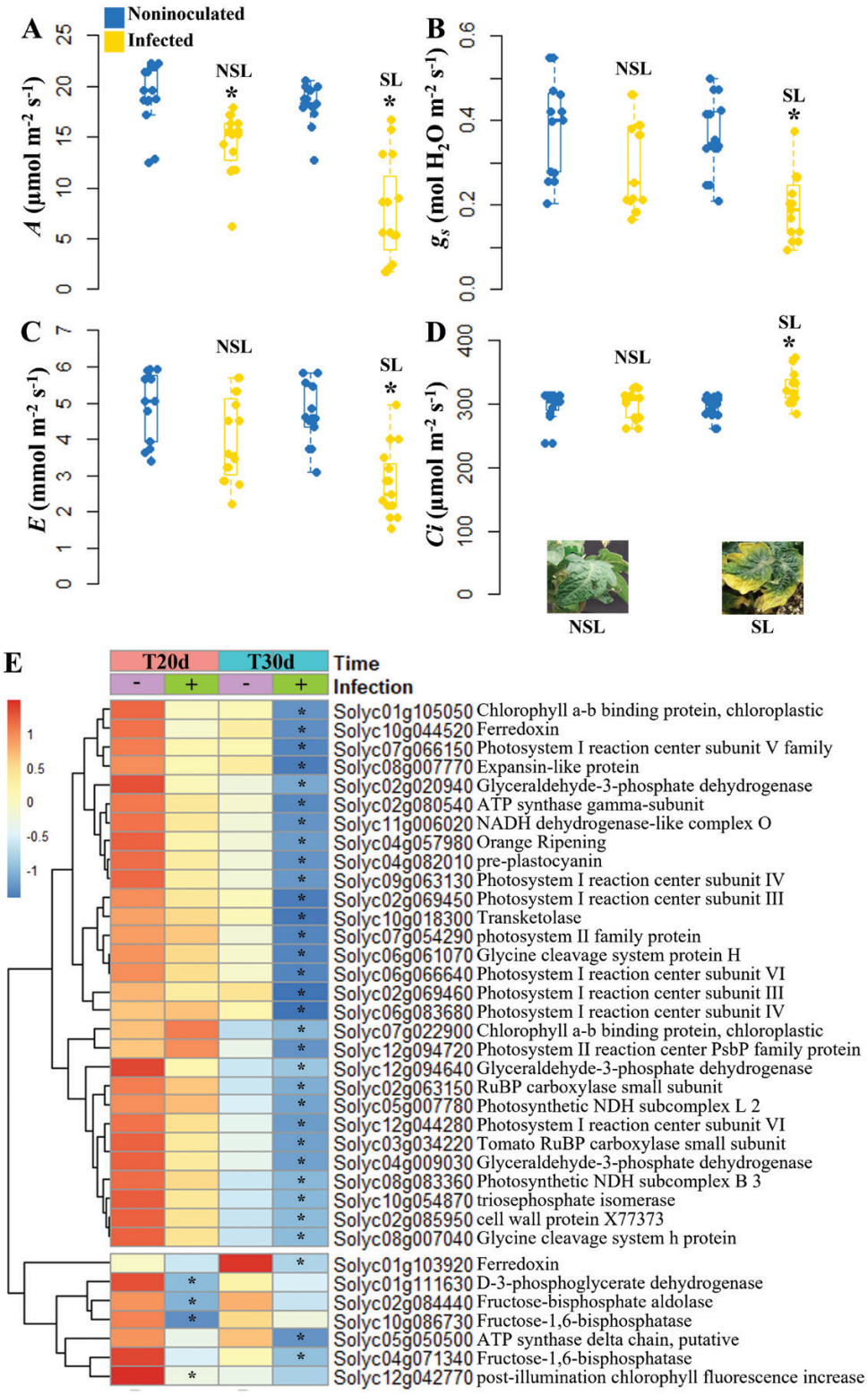

Fig. 3. Leaf gas exchange parameters and photosynthesis-related gene expression in response to infection of tomato Micro-Tom (MT) plants by the S-biotype of *Moniliophthora perniciosa*. (A) Net photosynthetic rate (*A*), (B) stomatal conductance (g_s), (C) transpiration rate (*E*), and (D) Intercellular CO_2 concentration (*Ci*) in the non-symptomatic leaf (NSL, non-chlorotic) and symptomatic leaf (SL, chlorotic)—the second and third fully expanded leaf, respectively—from infected plants, compared with the corresponding leaves from non-inoculated plants at 25 dai (n=10). In each boxplot, the middle line represents the median value, the upper and lower bars correspond to the first and third quartiles, respectively, and the whiskers represent 1.5 times the interquartile range. Statistically significant differences between infected and non-inoculated control plants were determined by the *t*-test and are indicated with asterisks (*P<0.05). The image inserts of leaves in (D) represent NSL and SL in (A–C) and Fig. 4A. (E) Heatmap of differentially expressed genes associated with photosynthesis in stems from non-inoculated or infected MT plants at 20 dai and 30 dai determined by RNA-seq, with clustering analysis according to the expression profiles obtained via the cuttree function in R (4.0.0). Genes with FDR ≤0.01 (1%) and fold change ≥2 were considered differentially expressed and are indicated with asterisks. The scale bar represents *z*-score-transformed TPM values (n=5).

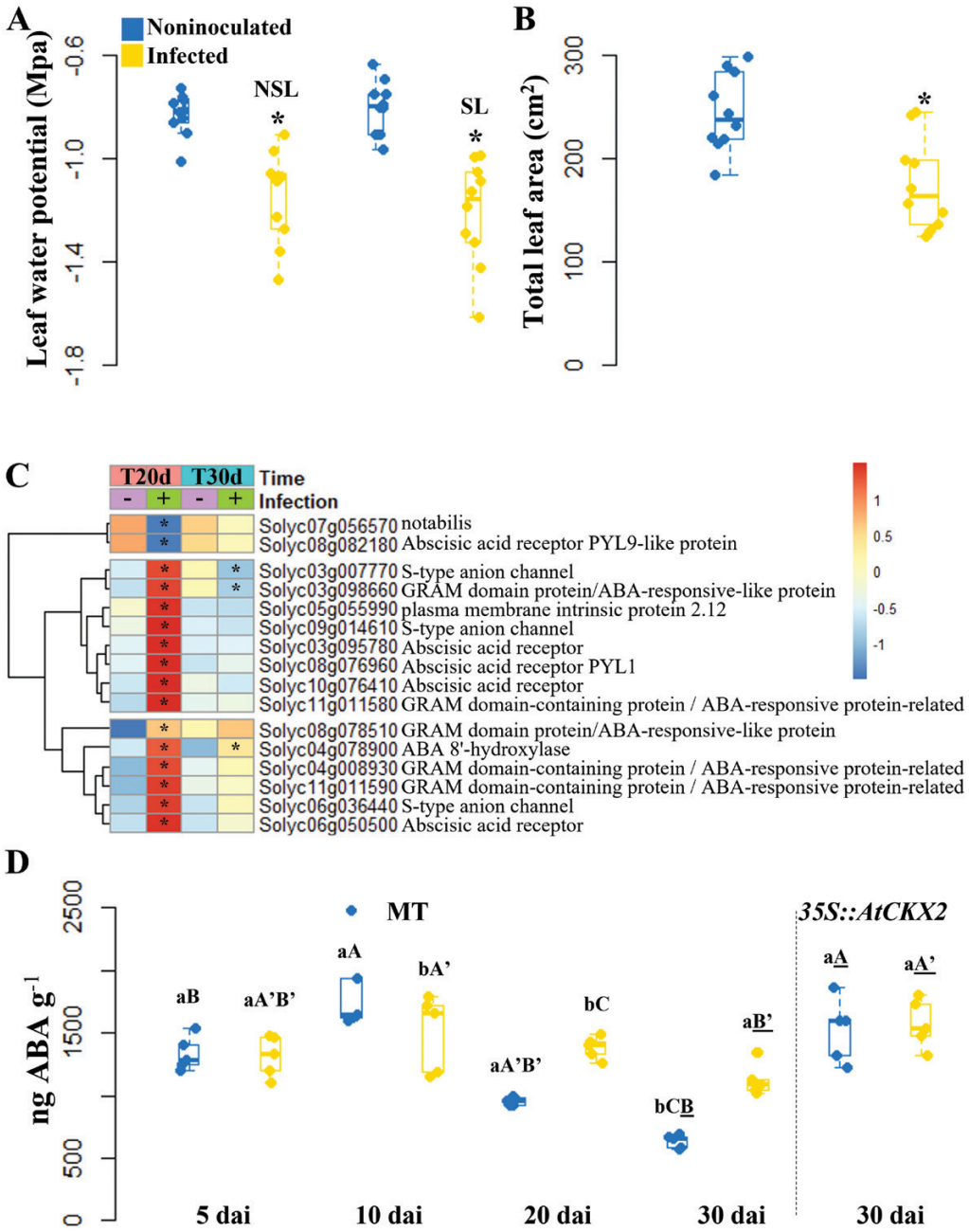

Fig. 4. Determination of water stress- and ABA-related gene expression and quantification in the stem and leaves of tomato Micro-Tom (MT) plants infected with the S-biotype of *Moniliophthora perniciosa*. (A) Water potential of the third expanded leaf without symptoms (non-chlorotic; NSL) or with symptoms (chlorotic; SL) from infected plants compared with the corresponding leaves from non-inoculated plants at 35 dai (n=10). (B) Total leaf area from non-inoculated or infected MT plants at 35 dai (n=10). In each boxplot, the middle line represents the median value, the upper and lower bars correspond to the first and third quartiles, respectively, and the whiskers represent 1.5 times the interquartile range. Statistically significant differences between infected and non-inoculated control plants were determined by the t-test and are indicated with asterisks (*P<0.05) (C) Heatmap of differentially expressed genes associated with abscisic acid (ABA) metabolism determined by RNA-seq in stems from non-inoculated or infected MT plants at 20 dai and 30 dai. Genes with FDR ≤0.01 (1%) and fold change ≥2 were considered differentially expressed and are indicated with asterisks. The scale bar represents z-score-transformed TPM values (n=5). (D) Quantification of ABA in stems from non-inoculated or infected MT plants at 5, 10, 20, and 30 dai, and in non-inoculated or inoculated transgenic *35S::AtCKX2* MT plants overexpressing an Arabidopsis cytokinin oxidase gene at 30 dai (n=5). Statistically significant differences (P<0.05) were determined by two-way ANOVA followed by the Tukey test. Different lowercase letters indicate mean significant differences between inoculated or non-inoculated plants within the MT or *35S::AtCKX2* genotypes at each time point; different uppercase letters indicate mean significant differences among time points within non-inoculated MT; different uppercase letters with ' indicate mean significant differences among time points within inoculated MT; different underlined uppercase letters indicate mean significant differences between non-inoculated MT and *35S::AtCKX2* genotypes at 30 dai; different underlined uppercase letters with ' indicate mean significant differences between inoculated MT and *35S::AtCKX2* plants at 30 dai.

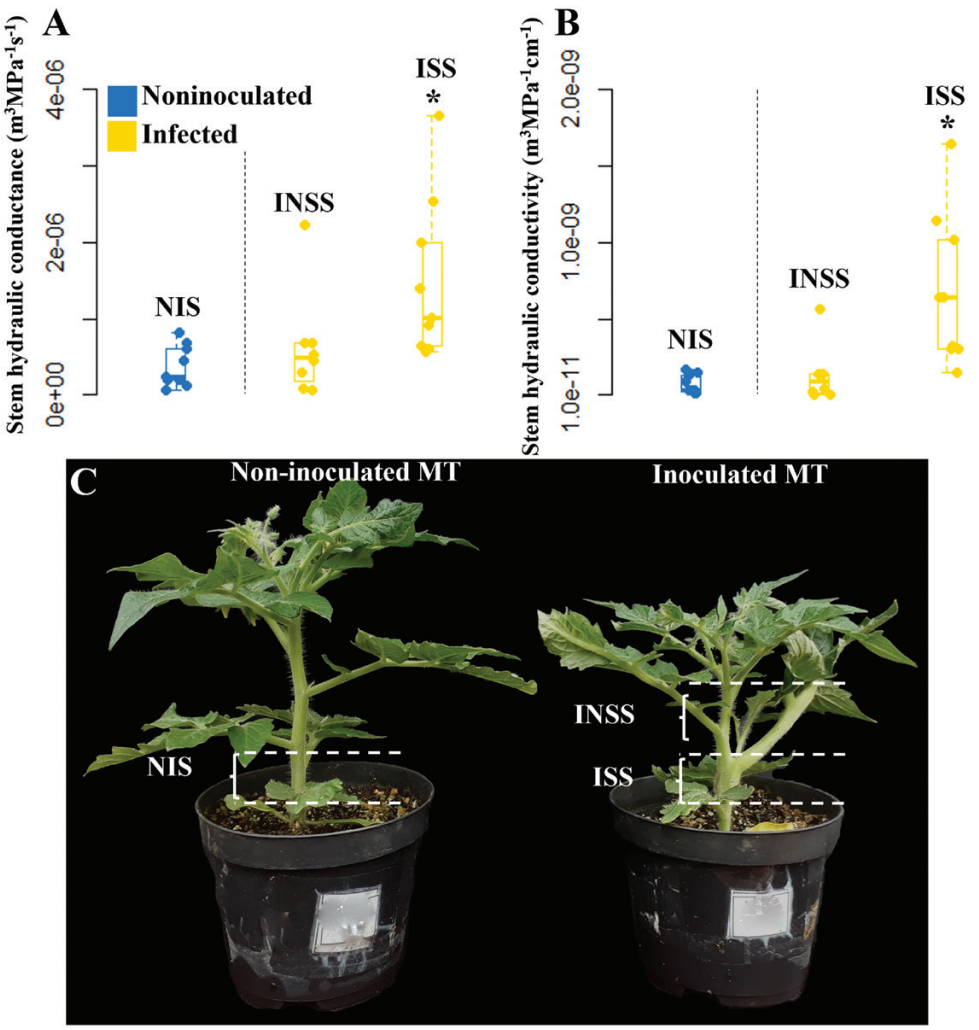

Fig. 5. Water conductance through the stem of tomato Micro-Tom (MT) plants infected with the S-biotype of *Moniliophthora perniciosa*. (A) Hydraulic conductance (m^3 MPa^{-1} s^{-1}) and (B) hydraulic conductivity (m^3 MPa^{-1} cm^{-1}) in non-symptomatic stems (INSS) or symptomatic stems (swollen region; ISS) from infected MT plants, or stems at the corresponding location from non-inoculated MT plants (NIS), at 35 dai (n=9). In each boxplot, the middle line represents the median value, the upper and lower bars correspond to the first and third quartiles, respectively, and the whiskers represent 1.5 times the interquartile range. Statistically significant differences between infected and non-inoculated control plants were determined by the-t test and are indicated with asterisks (*P<0.05). (C) Examples of non-inoculated (left) and inoculated (right) MT plants used for water conductance estimations.

Changes in metabolite accumulation in response to infection corroborate the development of a nutrient sink

We conducted a metabolic analysis of stems of infected MT plants compared with non-inoculated plants by gas chromatography coupled to time-of-flight mass spectrometry (GC-TOF-MS). Overall, we detected 54 metabolites associated with primary metabolism (Supplementary Table S2). Principal component analysis was performed to assess variability among samples from infected or non-inoculated plants at 4, 10, and 20 dai (Supplementary Fig. S6). Principal component 1 grouped the samples according to the developmental stage (Supplementary Fig. S6; Supplementary Table S3).

A significant change in the relative accumulation of 29 metabolites occurred in MT stems in response to infection at 4, 10, or 20 dai (Fig. 7A, B; Supplementary Fig. S7). The TCA intermediate fumarate, which might be related to carbon storage, accumulated at 20 dai (Fig. 7A). Sugars including fructose, gulose, and sorbose/tagatose (Fig. 7A) accumulated at 20 dai. Serine, glutamate, and β-alanine contents increased in infected tissues, while proline and phenylalanine contents were reduced (Fig. 7B). Metabolites related to cell wall modification, such as myo-inositol-1-phosphate, glucuronate, and threonate, also accumulated (Fig. 7C).

Swollen stems of infected MT take up ^{14}C-glucose, with a possible role for cytokinin

To investigate whether the swollen stem of infected MT plants indeed acts as a sugar sink, we applied ^{14}C-glucose

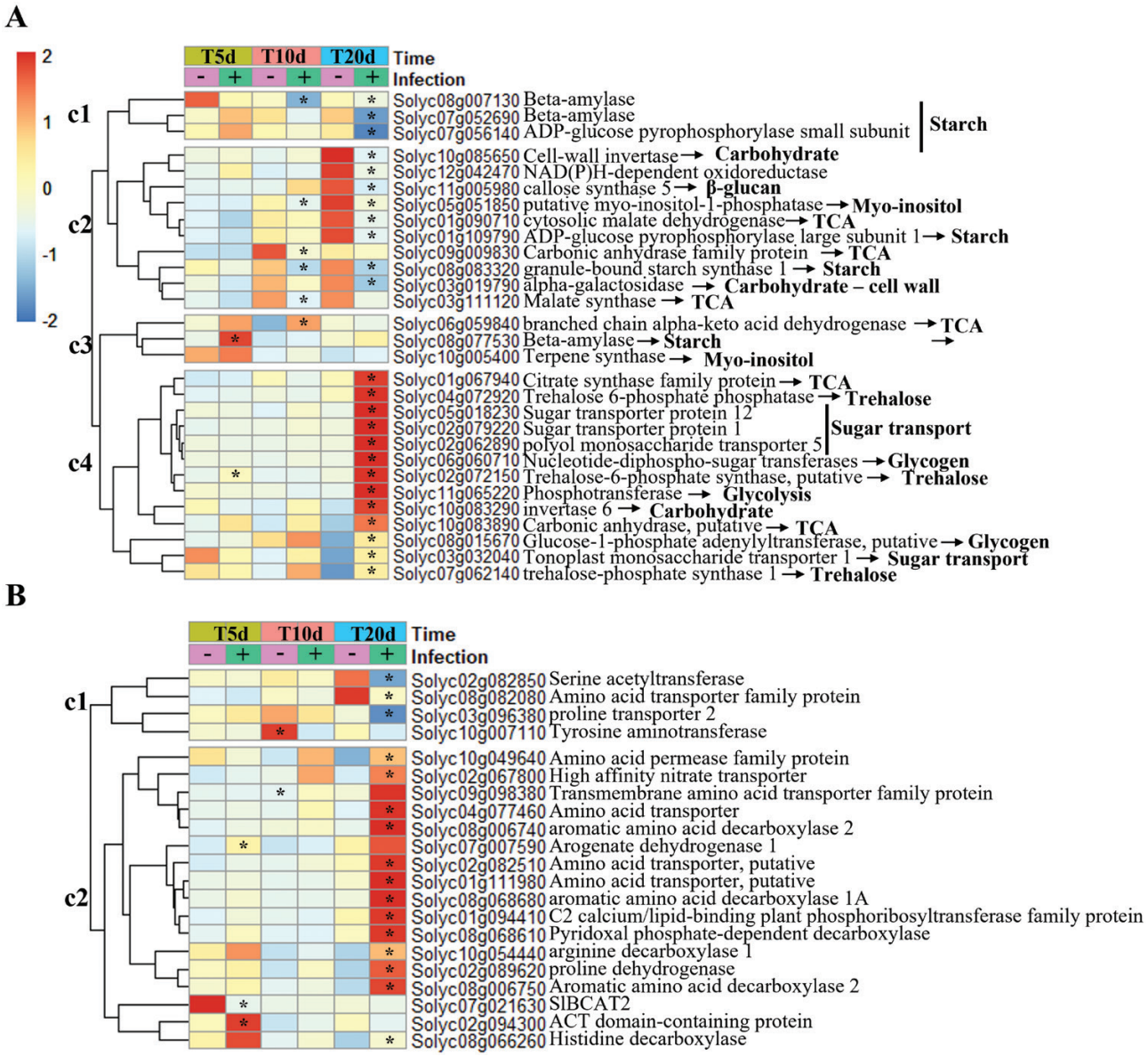

Fig. 6. Changes in the expression of genes associated with plant primary metabolism in response to infection of tomato Micro-Tom (MT) plants with the S-biotype of *Moniliophthora perniciosa*, determined by RNA-seq analysis. (A) Heatmap of differentially expressed genes (DEGs) associated with carbohydrate metabolism during infection at 5, 10, or 20 dai; (B) heatmap of DEGs associated with amino acid metabolism in stems from non-inoculated or infected MT plants, with clustering analysis according to the expression profiles obtained via the cuttree function in R (4.0.0). Genes with FDR ≤0.01 (1%) and fold change ≥2 were considered differentially expressed and are indicated with asterisks (n=5). The scale bar represents z-score-transformed TPM values.

to the first leaf above the inoculation site and to the corresponding leaf of non-inoculated plants at 4, 10, and 20 dai (Fig. 7D; Supplementary Fig. S8). ^{14}C-specific radioactivity was significantly higher in infected stems than in non-inoculated stems, corroborating the occurrence of a sugar sink, only at 20 dai (Fig. 7D). No significant difference was observed for the roots and leaves of infected plants at 20 dai (Fig. 7D) or for stems, roots, and leaves at 4 dai and 10 dai (Supplementary Fig. S8A, B).

We then applied ^{14}C-glucose to the low-cytokinin *35S::AtCKX2* line. Infected *35S::AtCKX2* plants showed no significant differences in ^{14}C-glucose translocation towards the stem or any other organs compared with non-inoculated *35S::AtCKX2* plants at 4, 10, or 20 dai (Fig. 7E; Supplementary Figs S8C, D, S9).

Application of 20 mM BA to the shoot apices and axillary buds of MT plants promoted stem thickening, loss of apical dominance, and a reduction in root biomass, somewhat mimicking

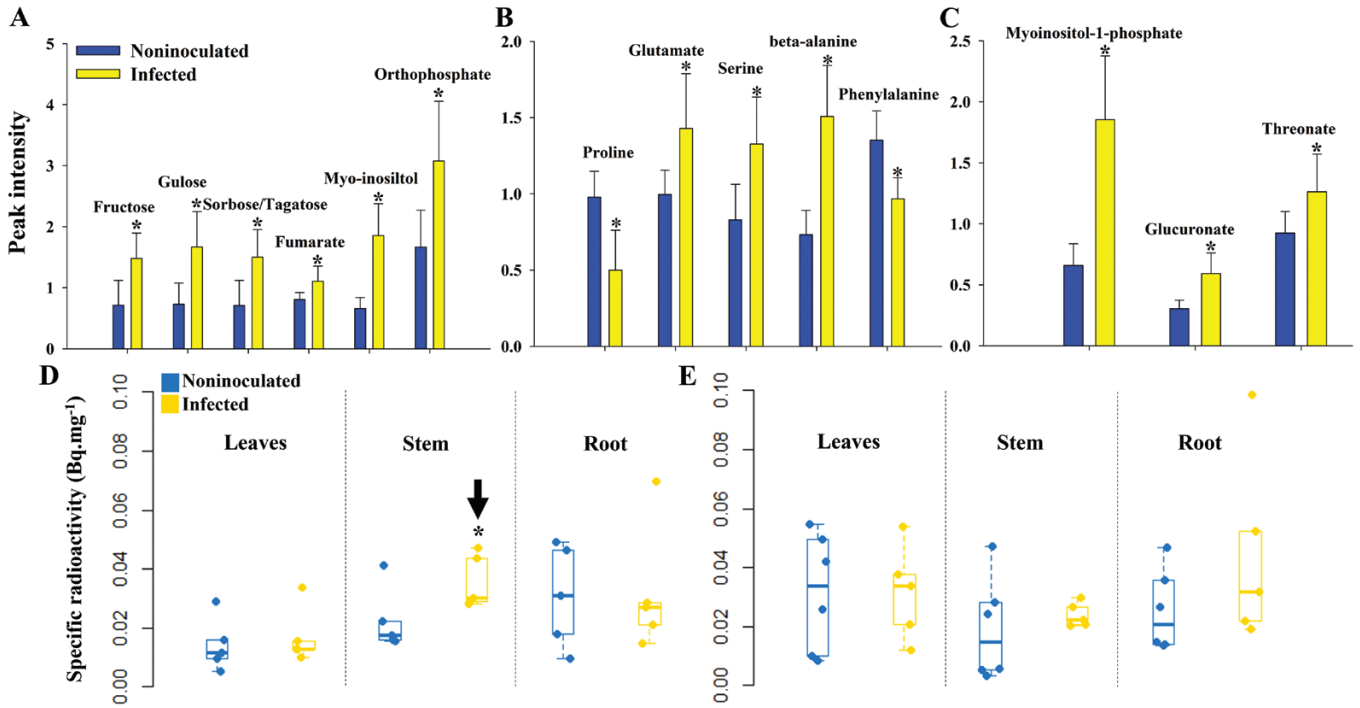

Fig. 7. Relative changes in metabolite levels in stems and ^{14}C translocation to organs of tomato Micro-Tom (MT) plants infected with the S-biotype of *Moniliophthora perniciosa*. (A–C) Mean peak intensity normalized by total ion count and sample mass ±SE identified by GC-TOF-MS (n=6): (A) carbohydrates and other metabolites possibly involved in sink induction at the site of infection; (B) amino acids; (C) metabolites related to cell wall modification with significant changes in stems from non-inoculated or infected plants at 20 dai. Statistically significant differences between infected and non-inoculated control plants at the same time point were determined by the t-test and are indicated with asterisks (*P<0.05). (D, E) ^{14}C-glucose translocation measured by specific activity (Bq mg^{-1}) in leaves, stem, or roots, applied at the first expanded leaf of (D) non-inoculated or infected MT plants; or (E) non-inoculated or inoculated MT transgenic line *35S::AtCKX2* plants at 20 dai (n=5). In each boxplot, the middle line represents the median value, the upper and lower bars correspond to the first and third quartiles, respectively, and the whiskers represent 1.5 times the interquartile range. Statistically significant differences between infected and non-inoculated plants in the same plant organ were determined by the t-test and are indicated with asterisks (*P<0.05).

the symptoms of infected MT plants (Supplementary Fig. S10A–D) (Costa *et al.*, 2021). When ^{14}C-glucose was applied to plants treated with BA, the detection of ^{14}C-radioactivity increased in stems and leaves at 5, 10, and 20 daa (Supplementary Fig. S10E–G) and in roots at 10 and 20 daa (Supplementary Fig. S10F, G) compared with mock-treated plants.

Sink development at the infection site may divert carbon resources towards secondary cell wall formation

We evaluated the expression of DEGs involved in cell wall deposition and modification in infected and non-inoculated plants. In the vascular tissue, xylem cells (e.g. tracheary elements and xylary fibres) deposit high amounts of SCWs. We observed the up-regulation of several genes involved in diverse aspects of cell wall deposition and modification, especially at 20 dai (Fig. 8A). Several of these genes encode enzymes involved in the biosynthesis of cellulose (e.g. cellulose synthase, COBRA) and hemicellulose (e.g. xyloglucan endotransglucosylase, cellulose synthase-like, glycosyltransferases), the biosynthesis of nucleotide sugars required for cell wall polysaccharide biosynthesis (e.g. UDP-glucose epimerase, UDP-glucunorate-4-epimerase, UDP-xylose synthase), and cell wall modification (e.g. endoglucanases, pectinesterases, glycosyl hydrolases, expansins) (Fig. 8A). Some cyclins were also up-regulated at 20 dai (Supplementary Fig. S11).

We determined changes in the expression of genes associated with the phenylpropanoid pathway, particularly with lignin metabolism, another major component of SCWs. Several genes associated with the phenylpropanoid biosynthetic pathway were up-regulated in infected stems, especially at 20 dai (Fig. 8B). We found genes involved in various aspects of lignin metabolism, including transcriptional regulation (e.g. LOB, orthologous to AtLOB15, and MYBs, orthologous to MYB11/12/13/14; Supplementary Fig. S12), biosynthesis (e.g. CCR and CAD, orthologous to AtCAD4/5; Supplementary Fig. S13), and polymerization (e.g. peroxidases, orthologous to AtPRX9; Supplementary Fig. S14) (Fig. 8B). The up-regulation of lignin-related genes at 20 dai was accompanied by the down-regulation of secondary-metabolism-related genes in infected MT plants, including those involved

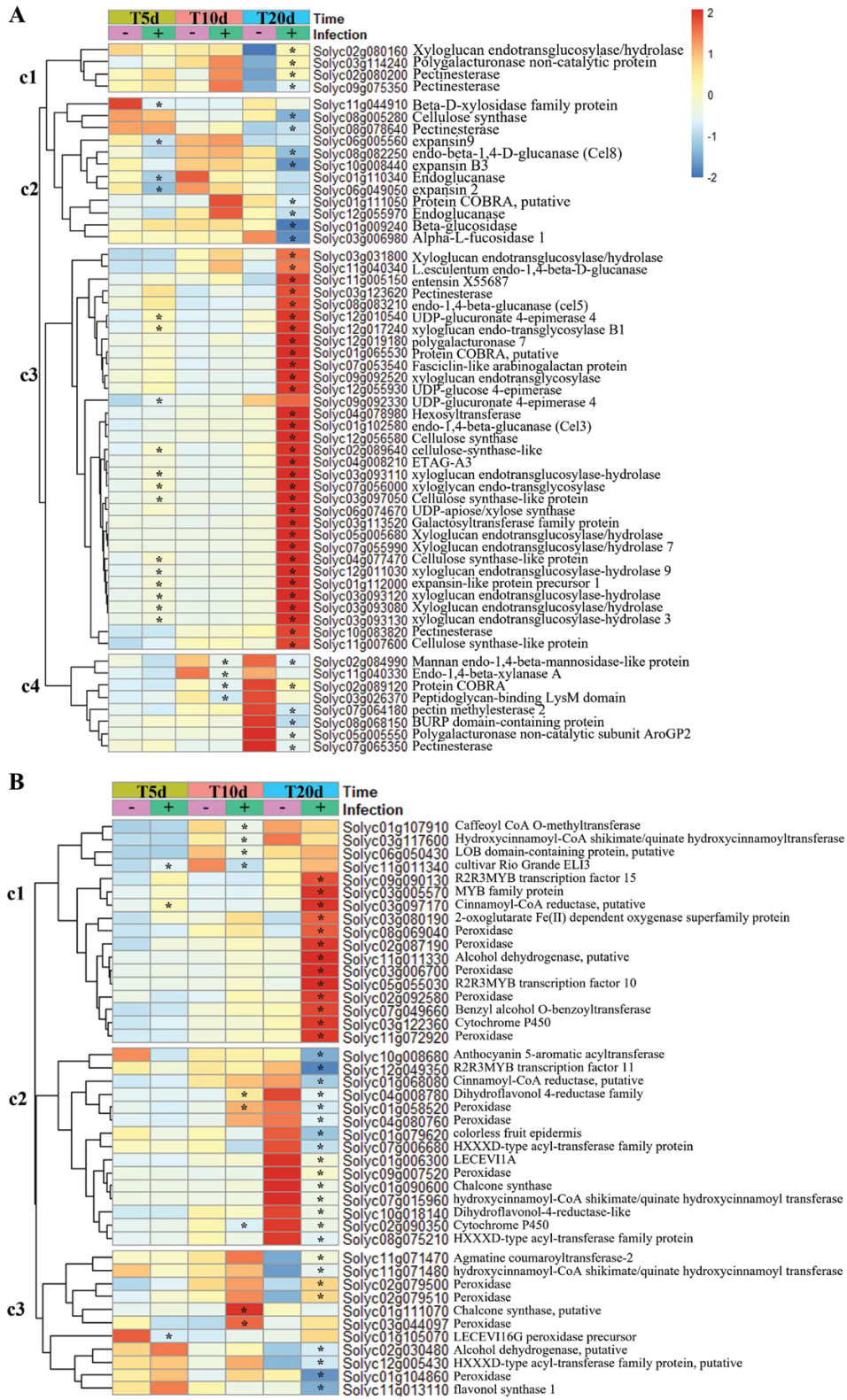

Fig. 8. Changes in the expression of genes associated with secondary cell wall metabolism in stems of tomato Micro-Tom plants infected with the S-biotype of *Moniliophthora perniciosa*. Heatmaps of differentially expressed genes associated with (A) cell wall and (B) phenylpropanoid metabolism in stems of non-inoculated or infected MT plants at 5, 10, or 20 dai determined by RNA-seq. Data were clustered according to the expression profiles analysed via the cuttree function in R (4.0.0) (n=5). Genes with FDR ≤0.01 (1%) and fold change ≥2 were considered differentially expressed and are indicated with asterisks. The scale bar represents z-score-transformed TPM values.

in flavonoid transcriptional regulation (e.g. MYBs) and biosynthesis (e.g. chalcone synthase, orthologous to AtLAP5; flavonol synthase; dihydroflavonol 4-reductases, orthologous to AtFLS1/3; anthocyanin acyltransferase, orthologous to AtDLR1; (Supplementary Fig. S15; Fig. 8B), as well as alkaloid and isoprenoid biosynthesis (Supplementary Fig. S16).

We further compared the transcriptional profile of genes related to cell wall and phenylpropanoid metabolism in MT and *35S::AtCKX2* plants at 30 dai (Fig. 9). Inoculated *35S::AtCKX2* plants did not exhibit the up-regulation of genes related to cell wall deposition and modification that was evident in MT plants (Fig. 9A). Other SCW- and lignin-related genes were up-regulated in stems of infected MT plants at 30 dai, including master regulators of the NAC (XND1, orthologous to AtXND1; Supplementary Fig. S17) and MYB family (MYB46), MYB transcription factors, the lignin biosynthesis gene 4-Coumarate 3-hydroxylase, and several monolignol oxidases (e.g. peroxidases and laccases, orthologous to AtLAC1/6; Supplementary Fig. S17; Fig. 9B). Importantly, these genes were not up-regulated in *35S::AtCKX2* plants at 30 dai (Fig. 9B).

To evaluate whether the up-regulation of SCW- and lignin-related genes was accompanied by changes in SCW contents, we measured the content of lignin in stems of infected and non-inoculated plants (Fig. 9C) and performed histochemical analysis for lignin staining at 30 dai (Fig. 9D). We observed that lignin contents were significantly higher in infected stems than in non-inoculated stems (Fig. 9C), and phloroglucinol–HCl staining indicated that there was more lignin deposition in infected stems in the hypertrophic growth of the vascular tissue (Fig. 9D; Supplementary Fig. S18).

To evaluate whether the increase in SCW/lignin contents in infected stems of MT could benefit the pathogen, we verified the expression of *M. perniciosa* genes with a presumed role in lignin degradation using the WBD Transcriptome Atlas (Teixeira *et al.*, 2014). We found 29 *M. perniciosa* laccases expressed during infection of cacao, with five (MP16486, MP14660, MP12873, MP07567, MP09646) (Supplementary Fig. S19) being preferentially expressed at the advanced necrotrophic stage of infection of cacao and in *in vitro* dikaryotic mycelium. A phylogenetic tree built with the complete laccase family of *M. perniciosa* and other characterized laccases from ligninolytic fungi showed the clustering of some of the *M. perniciosa* laccases preferentially expressed during the necrotrophic stage with fungal laccases recognized to degrade lignin (Supplementary Fig. S20).

Discussion

It is well established that WBD severely reduces cacao yield, but the cause of yield losses is poorly understood and pod rot is assumed to be the major reason for yield reduction (Purdy and Schmidt, 1996). However, it has been proposed that the general debilitation of trees culminates in yield losses (Teixeira *et al.*, 2014). The consequences of *M. perniciosa* infection on the physiology of cacao, a perennial tree, have been difficult to estimate (Rudgard, 1986). The availability of the S-biotype of *M. perniciosa*, which infects MT, allows the use of this model to fully investigate pathogenesis (Deganello *et al.*, 2014). Previously, we demonstrated a role for cytokinins in mediating symptom development during *M. perniciosa* infection of MT (Costa *et al.*, 2021). Here, we investigated the physiological and metabolic consequences of infection, proposing that the symptoms result from the formation of a novel and strong nutrient sink at the infection site while inducing SCW and lignin deposition (Supplementary Fig. S21).

Moniliophthora perniciosa infection of MT decreased the whole plant fruit yield (Fig. 2A, B), reduced the number of flowers in anthesis, and repressed genes related to flowering (Supplementary Fig. S3A, B), which might result from the lack of carbohydrates (Gibson *et al.*, 2005) and hormonal imbalance (Matías-Hernández *et al.*, 2016). Infected plants exhibited decreased root biomass but not primary root length (Fig. 2C, D), suggesting a negative effect on lateral root formation, presumably affecting nutrient and water uptake (Muller *et al.*, 2019). It is possible that a hormonal imbalance or nutrient deprivation might be affecting the root development (Celenza *et al.*, 1995; Liu *et al.*, 2017; Michniewicz *et al.*, 2019).

We observed reduced A, g_s, and E in leaves of infected plants but an increase in Ci (Fig. 3A–D), suggesting that the reduced A may have derived from impairment in g_s and in the Calvin cycle (Rouhi *et al.*, 2007; Gago *et al.*, 2016). The down-regulation of photosynthesis-related genes at 30 dai (Fig. 3E) might be related to the accumulation of hexoses at the infection site (Berger *et al.*, 2004; Walters and McRoberts, 2006), and the decrease in A might have resulted from the diversion of nutrients to the infected stem (sink) (Berger *et al.*, 2007), leading to the chlorotic phenotype of symptomatic leaves (Supplementary Fig. S1H). Despite the general positive effect of cytokinins in photosynthesis (McIntyre *et al.*, 2021), cytokinin-inducing pathogens were reported to decrease the expression of photosynthesis-related genes at the site of infection (Bruce *et al.*, 2011; Gohlke and Deeken, 2014; Matei *et al.*, 2018). Studies in cacao have indicated a decrease in A during infection with *M. perniciosa* (Orchard and Hardwick, 1988; Scarpari *et al.*, 2005; Barau *et al.*, 2014; Teixeira *et al.*, 2014) but, to the best of our knowledge, a comprehensive evaluation of the physiological consequences of infection has not been reported. During infection, MT plants exhibited a decrease in leaf water potential (Fig. 4A), likely reducing the total leaf area (Fig. 4B) and prompting decreases in g_s, E, and some of the carbon assimilation (Chaves, 1991; Aguirrezabal *et al.*, 2006). Stomatal closure is commonly associated with ABA accumulation and remobilization under conditions of water stress (Acharya and Assmann, 2009; Dittrich *et al.*, 2019), reducing transpiration rates in leaves (Else *et al.*, 2001;

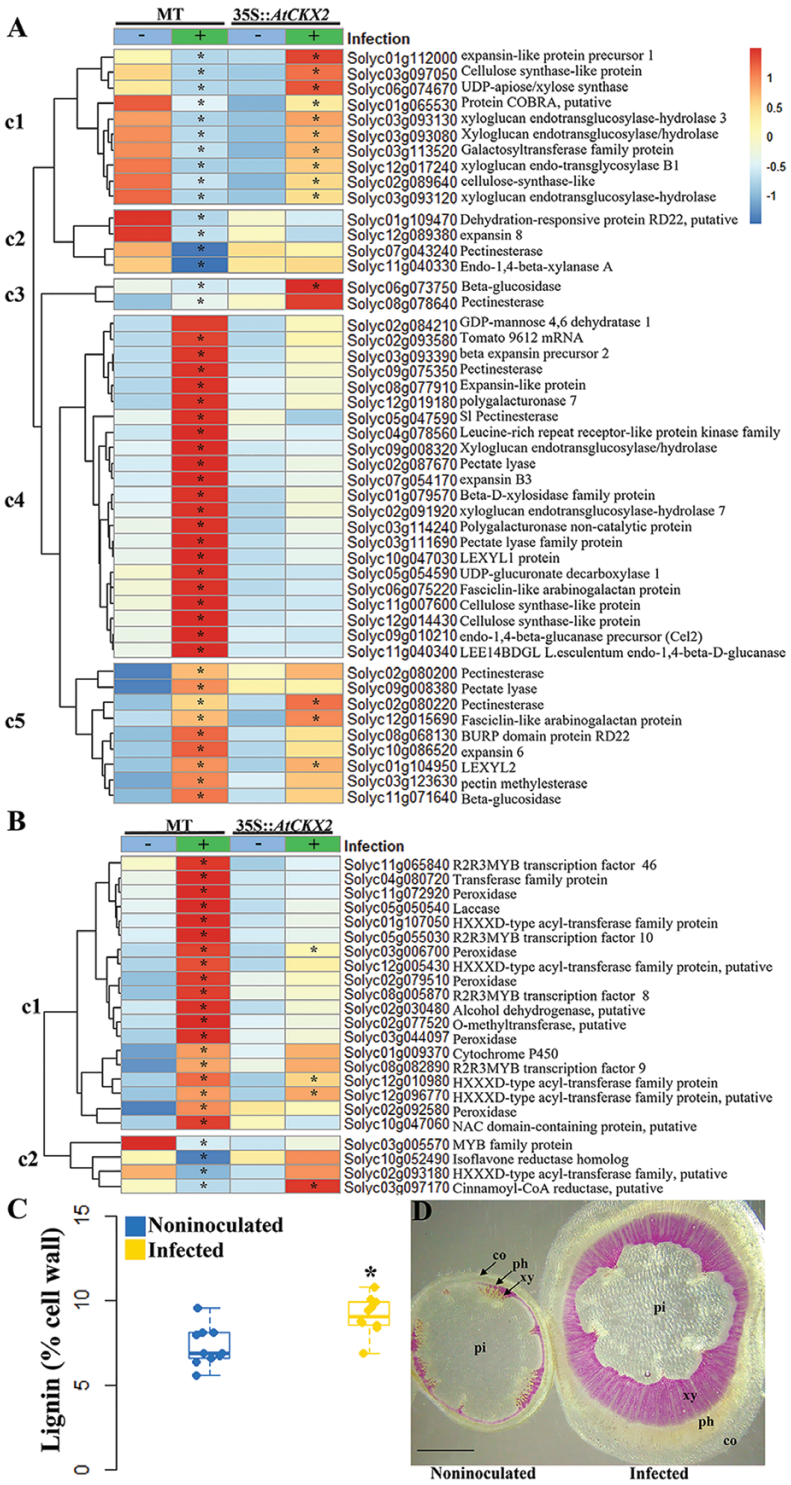

Fig. 9. Differential changes in the expression of genes related to secondary cell wall metabolism in stems of tomato Micro-Tom (MT) plants in comparison to the low-cytokinin transgenic line *35S::AtCKX2* infected or non-inoculated with *Moniliophthora perniciosa*. Heatmaps of differentially expressed genes associated with (A) cell wall and (B) phenylpropanoid metabolism in stems of non-inoculated or infected MT plants, or non-inoculated and inoculated MT-line *35S::AtCKX2* plants, at 30 dai, determined by RNA-seq analysis. Data were clustered according to the expression profiles analysed via the cuttree function in R (4.0.0) (n=5). Genes with FDR ≤0.01 (1%) and fold change ≥2 were considered differentially expressed and are indicated with asterisks. The scale bar represents z-score-transformed TPM values. (C) Quantification of lignin (% cell wall) in the stem of non-inoculated or infected MT plants at 30 dai (n=10). In each boxplot, the middle line represents the median value, the upper and lower bars correspond to the first and third quartiles, respectively, and the whiskers represent 1.5 times the interquartile range. Statistically significant differences between infected and non-inoculated corresponding control plants at the same time point were determined the by t-test and are indicated with asterisks (*P<0.05). (D) Histology of stem cross-sections of non-inoculated (left) or infected (right) MT plants stained with phloroglucinol–HCl. co, cortex; ph, phloem; pi, pith; xy, xylem. Bar=2mm.

Xiong and Nadal, 2020). Accordingly, we observed the up-regulation of genes that encode ABA receptors, anion channel proteins, and aquaporins (Fig. 4C), possibly as a protective mechanism against water stress. ABA levels did not decrease over time in infected stems, as occurred in non-inoculated stems (Fig. 4D). We propose that the reduction in root biomass caused by the infection of MT plants may interfere with water uptake, decreasing water potential in the leaves and possibly prompting ABA signalling (Li *et al.*, 2020), even with the increase of cytokinin (Costa *et al.*, 2021), which is an ABA antagonist (Cowan *et al.*, 1999). In other plant–pathogen interactions, the mutual increase of cytokinin and ABA levels to regulate sink formation has been reported (Bruce *et al.*, 2011; Gohlke and Deeken, 2014; Morrison *et al.*, 2017). Consistently, non-inoculated *35S::AtCKX2* plants showed higher levels of ABA compared with non-inoculated MT plants (Fig. 4D). It is possible that inoculation of *35S::AtCKX2* plants did not lead to the accumulation of ABA in comparison to non-inoculated plants, since these plants presented limited symptoms, without a sink establishment and evading a water stress response.

The swollen stems of MT plants in response to *M. perniciosa* infection result from the hypertrophic growth of xylem, phloem, and cortex tissues (Marelli *et al.*, 2009; Costa *et al.*, 2021), which is possibly induced by cytokinin and auxin imbalance (Aloni, 1995; Immanen *et al.*, 2016). The increase in water conductance/conductivity in the infected swollen MT stems (Fig. 5A, B) may be explained by the induction of xylogenesis (Costa *et al.*, 2021). Leafy gall caused by *R. fascians* in Arabidopsis promotes a hormonal imbalance and culminates in *de novo* vascularization to shunt water and nutrients to the infection site (Dolzblasz *et al.*, 2018), while *Picea glauca* branches parasitized by *Arceuthobium pusillum* form new vasculature to strengthen the organ sink, mediated by cytokinins (Logan *et al.*, 2013). Whether the increase in water translocation to infected MT stems is a fortuitous result of excessive xylogenesis or a key mechanism for infection remains to be determined.

Our results suggest that the infected swollen stem leads to the establishment of a nutrient sink. Previous work with cacao suggested that *M. perniciosa* infection induced sink establishment (Barau *et al.*, 2014; Teixeira *et al.*, 2014). Here, we observed the up-regulation of genes involved in sugar and nitrogen transport and catabolism (Fig. 6A, B) (Tegeder and Masclaux-Daubresse, 2018; Fichtner *et al.*, 2020*a*). The induction of *INVERTASE-6* is associated with the release of hexoses to the host apoplast (Proels and Roitsch, 2009), as proposed in cacao (Teixeira *et al.*, 2014) and other plant–pathogen interactions (Lemoine *et al.*, 2013; Veillet *et al.*, 2016; Pommerrenig *et al.*, 2020). The infection of *Pisum sativum* cotyledon with *R. fascians* increased N^6-(Δ^2-isopentenyl)adenine levels and induced the expression of cytokinin-responsive genes, sugar transporters, and invertases (*PsSWEET*, *PsSUT*, *CWIV*, *PsINV*), and the retention of the infected cotyledons as sink tissues (Dhandapani *et al.*, 2017). As cell-wall invertases are known to be induced by cytokinins (Walters and McRoberts, 2006), we propose that the increased concentrations of cytokinins in MT stems infected with *M. perniciosa* (Costa *et al.*, 2021) may explain the higher expression of *INVERTASE-6*. Application of cytokinins to *Chenopodium rubrum* suspension cells up-regulated the hexose transporter genes *CST2* and *CST3* and increased the uptake of ^{14}C-glucose (Ehneß and Roitsch, 1997). The significant increase in ^{14}C-glucose remobilization towards the infected stem (Fig. 7D) reinforces the suggestion of sink establishment. Inoculation of the low-cytokinin *35S::AtCKX2* line did not increase the translocation of ^{14}C-glucose towards the stem (Fig. 7E), whereas BA treatment of MT plants increased the translocation towards stems, leaves, and roots (Supplementary Fig. S10E–G), corroborating a role of cytokinin in regulating sugar partitioning to induce a sink at the infected stem.

We observed up-regulation of the sugar sensors *TPS* and *TPP* and a *PHOSPHOTRANSFERASE* orthologue of Arabidopsis HKX1 (Fichtner *et al.*, 2021), suggesting altered sugar signalling at the infected stem. TPS was suggested to coordinate the source–sink relationship by redirecting sucrose carbon into the TCA and to amino acid synthesis and by regulating the cell cycle (Figueroa *et al.*, 2016; Fichtner et al., 2020*a*, *b*). The induction of *STP1* (orthologue of Arabidopsis *STP1*) and *STP12* (orthologue of Arabidopsis *STP14*) corroborates sink establishment in the infected stem (Büttner, 2010; Sakr *et al.*, 2018). The infection of cabbage with the biotroph *P. brassicae* induced *BoSTP4b* and *BoSTP12*, suggesting an involvement in carbon partitioning in gall development (Zhang *et al.*, 2019*b*), while infection of wheat with *P. striiformis* f. sp. *tritici* (the causal agent of stripe rust disease) induced *TaSTP13*, possibly to accumulate hexoses to feed the pathogen (Huai *et al.*, 2020). Transcriptional analysis of the interaction of *M. perniciosa* with *T. cacao* revealed the up-regulation of hexose transporters in cacao (Teixeira *et al.*, 2014). In MT, hexose transporters may function in providing the high energy demanded for sink establishment (Horst *et al.*, 2010), as the pathogen grows at low density during biotrophic infection. Alternatively, hexose transporters could benefit the pathogen's consumption of hexoses (Teixeira *et al.*, 2014).

Metabolic analysis depicted an increase in the levels of fructose and other sugars (gulose, sorbose, and psicose) and some amino acids (glutamate and serine) in the infected stem (Fig. 7A, B; Supplementary Fig. S7), likely contributing to sink establishment and functioning as a signal to decrease the photosynthetic rates in leaves (Berger *et al.*, 2007). Although glucose did not accumulate, we presume that the induced phosphotransferase might be channelling glucose into the glycolytic pathway (Rojas *et al.*, 2014). During *Botrytis cinerea* infection of Arabidopsis, although a cell-wall invertase and several sugar transporters were up-regulated, reduced levels of hexoses were found, suggesting an increased activity of the glycolytic and respiration pathways to fuel plant defences (Veillet *et al.*, 2017). The infection of maize tissues with *U. maydis*, and of Arabidopsis with powdery mildew, caused the

up-regulation of genes related to glycolysis and the TCA cycle (Doehlemann *et al.*, 2008; Chandran *et al.*, 2010; Horst *et al.*, 2010), suggesting a flow of carbon to synthesize amino acids or to increase respiration to adapt to the high energy demand at the infection site. Here, we found increased fumarate contents, suggesting either the activation of the glycolytic and respiration pathways or carbon storage (Sweetlove *et al.*, 2010; Zell *et al.*, 2010).

We propose that the establishment of a nutrient sink at the infection site may involve the channelling of carbon skeletons towards SCW formation. This hypothesis is supported by the following: (i) hypertrophic growth of the vascular tissue (Costa *et al.*, 2021), which is enriched in SCWs, upon infection; (ii) up-regulation of genes encoding master switches of SCW deposition, which are known to regulate SCW synthesis and programmed cell death (Figs 8A, B, 9A, B) (Zhong *et al.*, 2007; Zhao *et al.*, 2008; Zhong and Ye, 2012); (iii) up-regulation of biosynthetic genes for all three major components of SCW (i.e. cellulose, hemicellulose, and lignin) (Figs 8A, B, 9A); (iv) up-regulation of MYB transcription factors known to specifically regulate lignin deposition (Chezem *et al.*, 2017; Kim *et al.*, 2020) and of monolignol oxidases (i.e. peroxidases and laccases) (Figs 8B, 9B); and (v) a decrease in phenylalanine (lignin precursor) (Fig. 7B) and an increase in lignin contents upon infection (Fig. 9C). Lignin deposition is known to occur in response to biotic stresses to reinforce the cell wall against pathogens (Cesarino, 2019). Here, we suggest that lignification in infected MT stems is part of the hypertrophic growth of the vascular tissue during the establishment of a nutrient sink at the site of infection. Whereas cytokinin treatment was shown to increase the expression of phenylpropanoid-related genes (Bhargava *et al.*, 2013; Tyagi *et al.*, 2021), xylem differentiation and SCW deposition were shown to be regulated by ABA via transcriptional and post-translational regulation of master switches of the NAC family (Ramachandran *et al.*, 2021; Liu *et al.*, 2021). In parallel, genes related to the biosynthesis of specialized metabolites involved in plant defence (e.g. flavonoids, alkaloids, and isoprenoids) were repressed, suggesting that the pathogen might disable potential protective pathways in the plant. The up-regulation of genes related to cell wall reinforcement and lignin biosynthesis was also observed in cacao infected with *M. perniciosa*, suggesting a host strategy to limit pathogen colonization (Teixeira *et al.*, 2014). Importantly, *35S::AtCKX2* plants did not show the up-regulation of SCW- and phenylpropanoid-related genes (Fig. 9A, B), suggesting a key role of cytokinins inducing sink establishment in mediating these responses. Thus, we propose that *M. perniciosa* induces the establishment of a nutrient sink via the accumulation of cytokinins at the infection site, along with the accumulation of ABA, contributing to the activation of xylem differentiation and SCW deposition.

Although it displays a pathogenic lifestyle, *M. perniciosa* belongs to the Marasmiaceae, which contains predominantly saprotrophic species (Lisboa *et al.*, 2020) with significant ligninolytic activity (Osono *et al.*, 2020). Moreover, *M. perniciosa* has been demonstrated to decompose cellulose and lignin *in vitro* (Lindeberg and Molin, 1949; Hedger *et al.*, 1987). Fungal laccases are major players in lignin degradation during wood decomposition (Janusz *et al.*, 2017). The genome of *M. perniciosa* contains genes encoding ligninolytic enzymes (e.g. manganese-dependent peroxidase and laccases) (Mondego *et al.*, 2008), and we found five laccases expressed in the dikaryotic mycelium and during the advanced necrotrophic stage of infection of cacao by the C-biotype of *M. perniciosa* (WBD Transcriptome Atlas) (Supplementary Fig. S19). It is possible that the accumulated lignin at the infection site could benefit *M. perniciosa* as an energy source in the saprotrophic phase, when the fungus grows abundantly (Sena *et al.*, 2014), and before facing other competing saprotrophs (Hedger *et al.*, 1987).

Thus, we propose that infection with *M. perniciosa* may induce the establishment of a cytokinin-mediated nutrient sink, SCW deposition, and accumulation of lignin at the infected stem. It is possible that the translocation of sugars and water to the symptomatic region, along with the reduction in root biomass, contributes to reducing photosynthesis and water status in leaves, possibly impairing plant development and reducing fruit yield. The overall metabolic and physiological disarrangement during *M. perniciosa* infection, demonstrated in tomato, likely contributes to the severe and prolonged impact of WBD in cacao production.

Supplementary data

The following supplementary data are available at *JXB* online.

Table S1. Annotation of MapMan BINs enriched for differentially expressed genes at 5, 10, 20, and 30 dai of tomato MT with the S-biotype of *M. perniciosa*.

Table S2. Metabolites detected by GC-TOF-MS in stems of tomato MT plants infected with the S-biotype of *M. perniciosa* or non-inoculated, analysed over the period of infection.

Table S3. Loadings of principal component analysis representing relative changes in metabolite levels in stems of tomato MT plants infected with the S-biotype of *M. perniciosa* or non-inoculated, analysed over the period of infection.

Fig. S1. Symptoms of tomato MT plants infected with the S-biotype of *M. perniciosa*.

Fig. S2. Representative images of the progression of symptoms of tomato MT plants infected with the S-biotype of *M. perniciosa*.

Fig. S3. Number of flowers after anthesis per plant and DEGs related to flowering in tomato MT plants infected with the S-biotype of *M. perniciosa*.

Fig. S4. Detection of *M. perniciosa* in stems or roots from infected tomato MT plants by DNA amplification.

Fig. S5. MapMan representation of DEGs of the Calvin cycle and light reactions in stems of tomato MT plants infected with the S-biotype of *M. perniciosa*.

Fig. S6. Principal component analysis scores plot representing relative changes in metabolite levels in stems of tomato MT plants infected with the S-biotype of *M. perniciosa*.

Fig. S7. Heatmap representing changes in all identified metabolites in stems of tomato MT plants infected with the S-biotype of *M. perniciosa*.

Fig. S8. Specific activity (Bq mg^{-1}) detected in leaves, stem, or root of tomato MT plants infected with the S-biotype of *M. perniciosa* after application of ^{14}C-glucose.

Fig. S9. Representative images of transgenic MT line *35S::AtCKX2* non-inoculated or inoculated with the S-biotype of *M. perniciosa*.

Fig. S10. Specific activity (Bq mg^{-1}) detected in leaves, stem, or root of tomato MT plants treated with 20 mM BA after application of ^{14}C-glucose.

Fig. S11. Heatmap of DEGs related to cell cycle metabolism in stems of tomato MT plants infected with the S-biotype of *M. perniciosa*.

Fig. S12. Comparative phylogenetic trees of Lateral organ boundaries (LOB) domain (LBD) and MYB transcription factors.

Fig. S13. Comparative phylogenetic tree constructed with cinnamyl alcohol dehydrogenase (CAD) enzymes from *Arabidopsis thaliana*, *Populus trichocarpa*, and tomato.

Fig. S14. Comparative phylogenetic tree constructed with peroxidase proteins from *Arabidopsis thaliana* and tomato.

Fig. S15. Comparative phylogenetic tree constructed with chalcone synthase, leucoanthocyanidin dioxygenase/anthocyanidin synthase, and dihydroflavonol-4-reductase/anthocyanidin reductase enzymes.

Fig. S16. Heatmap of DEGs related to secondary metabolism in stems of tomato MT plants infected with the S-biotype of *M. perniciosa*.

Fig. S17. Comparative phylogenetic tree constructed with No Apical Meristem, Arabidopsis transcription activation factor, and Cup-Shaped Cotyledon (NAC) transcription factors, 4-Coumarate 3-hydroxylase, and laccases.

Fig. S18. Histology of stem cross-sections of infected MT stained with phloroglucinol–HCl for lignin detection.

Fig. S19. Boxplots indicating the expression of five *M. perniciosa* laccase genes preferentially expressed at the necrotrophic stage of infection of *Theobroma cacao* shoot by the C-biotype of *M. perniciosa*.

Fig. S20. Comparative phylogenetic tree constructed with laccases from *M. perniciosa* and other fungi with ligninolytic function.

Fig. S21. Proposed hypothetical schematic model representing the physiological and metabolic changes in response to infection of MT plants by the S-biotype of *M. perniciosa*.

Acknowledgements

The authors are thankful for technical help from Dr Danielle Scotton and Dr Jamille Santos da Silva. The authors wish to thank the University of North Carolina High Throughput Sequencing Facility for support with the RNA-seq analysis and the Universitat Politécnica de Valência, Spain, for support with the hormonal analysis. Research was supported by LNBR–Brazilian Biorenewables National Laboratory (CNPEM/MCTIC) during the use of the Metabolomics open-access facility.

Author contributions

AF and DP designed the research project; DP, JLC, EMS, and VO performed experiments; DP analysed and interpreted the data; PJPLT, DMRP, and DP performed bioinformatic analysis; IC helped to analyse/interpret the SCW data; FBS, DC, JAA, GGC, RFP, RFO, EC, ILD, MLR, CC, VT, and IC contributed with analysis/reagents/materials/tools; DP and AF wrote the manuscript; AF supervised the project and experiments.

Conflict of interest

The authors have no conflicts of interest to declare.

Funding

This work was supported by the Fundação de Amparo à Pesquisa do Estado de São Paulo (FAPESP) through a Thematic Research Grant (16/10498-4), a Regular Research Grant (19/25597-0), and fellowships to DP (2018/18711-4), JLC (13/04309-6; BEPE 16/10524-5), EMS (17/17000-4). Additional support came from the Conselho Nacional de Desenvolvimento Científico e Tecnológico (CNPq) through research grants (471631/2013-2; 409681/2018-0) and a fellowship to DP (132376/2016-4).

Data availability

The data supporting the findings of this study are available from the corresponding author, Antonio Figueira, upon request.

References

Acharya BR, Assmann SM. 2009. Hormone interactions in stomatal function. Plant Molecular Biology **69**, 451–462.

Aguirrezabal L, Bouchier-Combaud S, Radziejwoski A, Dauzat M, Cookson SJ, Granier C. 2006. Plasticity to soil water deficit in *Arabidopsis thaliana*, dissection of leaf development into underlying growth dynamic and cellular variables reveals invisible phenotypes. Plant, Cell and Environment **29**, 2216–2227.

Albrecht T, Argueso CT. 2017. Should I fight or should I grow now? The role of cytokinins in plant growth and immunity and in the growth–defence trade-off. Annals of Botany **119**, 725–735.

Aloni R. 1995. The induction of vascular tissues by auxin and cytokinin. In: Davies PJ, ed. Plant hormones: physiology, biochemistry and molecular biology. Dordrecht: Kluwer Academic, 531–546.

Andrews S. 2010. FastQC, a quality control tool for high throughput sequence data. https://www.bioinformatics.babraham.ac.uk/projects/fastqc/. Accessed 5 January 2017.

Artero AS, Silva JQ, Albuquerque PSB, Bressan EA, Leal GA, Jr, Sebenn AM, Griffith GW, Figueira A. 2017. Spatial genetic structure and dispersal of the cacao pathogen *Moniliophthora perniciosa* in the Brazilian Amazon. Plant Pathology **66**, 912–923.

Atkinson CJ, Else MA, Taylor L, Dover CJ. 2003. Root and stem hydraulic conductivity as determinants of growth potential in grafted trees of apple*Malus pumila* Mill. Journal of Experimental Botany **54**, 1221–1229.

Barau J, Grandis A, Carvalho VMA, Teixeira GS, Zaparoli GHA, do Rio MCS, Rincones J, Buckeridge MS, Pereira GAG. 2014. Apoplastic and intracellular plant sugars regulate developmental transitions in witches' broom disease of cacao. Journal of Experimental Botany **66**, 1325–1337.

Bhargava A, Clabaugh I, To JP, Maxwell BB, Chiang YH, Schaller GE, Loraine A, Kieber JJ. 2013. Identification of cytokinin-responsive genes using microarray meta-analysis and RNA-Seq in Arabidopsis. Plant Physiology **162**, 272–294.

Berger S, Papadopoulos M, Schreiber U, Kaiser W, Roitsch T. 2004. Complex regulation of gene expression, photosynthesis and sugar levels by pathogen infection in tomato. Physiologia Plantarum **122**, 419–428.

Berger S, Sinha AK, Roitsch T. 2007. Plant physiology meets phytopathology, plant primary metabolism and plant–pathogen interactions. Journal of Experimental Botany **58**, 4019–4026.

Bolger AM, Lohse M, Usadel B. 2014. Trimmomatic, a flexible trimmer for Illumina 677 sequence data. Bioinformatics **30**, 2114–2120.

Bruce SA, Saville BJ, Emery RN. 2011. *Ustilago maydis* produces cytokinins and abscisic acid for potential regulation of tumor formation in maize. Journal of Plant Growth Regulation **30**, 51–63.

Büttner M. 2010. The *Arabidopsis* sugar transporter (AtSTP) family, an update. Plant Biology **12**, 35–41.

Carvalho RF, Campos ML, Pino LE, Crestana SL, Zsögön Z, Lima JE, Benedito VA, Peres LEP. 2011. Convergence of developmental mutants into a single tomato model system, 'Micro-Tom' as an effective toolkit for plant development research. Plant Methods **71**, 18.

Celenza JJ, Grisafi PL, Fink GR. 1995. A pathway for lateral root formation in *Arabidopsis thaliana*. Genes & Development **9**, 2131–2142.

Cesarino I. 2019. Structural features and regulation of lignin deposited upon biotic and abiotic stresses. Current Opinion in Biotechnology **56**, 209–214.

Chanclud E, Kisiala A, Emery NRJ, Chalvon V, Ducasse A, Romiti-Michel C, Gravot A, Kroj T, Morel JB. 2016. Cytokinin production by the rice blast fungus is a pivotal requirement for full virulence. PLoS Pathogens **12**, e1005457.

Chanclud E, Morel JB. 2016. Plant hormones: a fungal point of view. Molecular Plant Pathology **17**, 1289–1297.

Chandran D, Inada N, Hather G, Kleindt CK, Wildermuth MC. 2010. Laser microdissection of *Arabidopsis* cells at the powdery mildew infection site reveals site-specific processes and regulators. Proceedings of the National Academy of Sciences USA **107**, 460–465.

Chaves MM. 1991. Effects of water deficit on carbon assimilation. Journal of Experimental Botany **42**, 1–16.

Chezem WR, Memon A, Li FS, Weng JK, Clay NK. 2017. SG2-type R2R3-MYB transcription factor MYB15 controls defense-induced lignification and basal immunity in Arabidopsis. The Plant Cell **29**, 1907–1926.

Costa JL, Paschoal D, da Silva EM, *et al*. 2021. *Moniliophthora perniciosa*, the causal agent of witches' broom disease of cacao, interferes with cytokinin metabolism during infection of Micro-Tom tomato and promotes symptom development. New Phytologist **231**, 365–381.

Cowan AK, Cairns AL, Bartels-Rahm B. 1999. Regulation of abscisic acid metabolism: towards a metabolic basis for abscisic acid-cytokinin antagonism. Journal of Experimental Botany **50**, 595–603.

Cuadros-Inostroza A, Caldana C, Redestig H, Kusano M, Lisec J, Peña-Cortés H, Willmitzer L, Hannah MA. 2009. TargetSearch - a Bioconductor package for the efficient preprocessing of GC-MS metabolite profiling data. BMC Bioinformatics **10**, 428.

Davies CR, Wohlgemuth F, Young T, Violet J, Dickinson M, Sanders JW, Vallieres C, Avery SV. 2021. Evolving challenges and strategies for fungal control in the food supply chain. Fungal Biology Reviews **36**, 1526.

Deganello J, Leal GA, Jr, Rossi ML, Peres LEP, Figueira A. 2014. Interaction of *Moniliophthora perniciosa* biotypes with Micro-Tom tomato: a model system to investigate the witches' broom disease of *Theobroma cacao*. Plant Pathology **63**, 1251–1263.

Dhandapani P, Song J, Novak O, Jameson PE. 2017. Infection by *Rhodococcus fascians* maintains cotyledons as a sink tissue for the pathogen. Annals of Botany **119**, 841–852.

Dittrich M, Mueller HM, Bauer H, *et al*. 2019. The role of *Arabidopsis* ABA receptors from the PYR/PYL/RCAR family in stomatal acclimation and closure signal integration. Nature Plants **5**, 1002–1011.

Doehlemann G, Wahl R, Horst RJ, *et al*. 2008. Reprogramming a maize plant: transcriptional and metabolic changes induced by the fungal biotroph *Ustilago maydis*. The Plant Journal **56**, 181–195.

Dolzblasz A, Banasiak A, Vereecke D. 2018. Neovascularization during leafy gall formation on *Arabidopsis thaliana* upon *Rhodococcus fascians* infection. Planta **247**, 215–228.

Doyle JJ, Doyle JL. 1990. A rapid total DNA preparation procedure for fresh plant tissue. Focus **12**, 13–15.

Ehlert C, Maurel C, Tardieu F, Simmoneau T. 2009. Aquaporin-mediated reduction in maize root hydraulic conductivity impacts cell turgor and leaf elongation even without changing transpiration. Plant Physiology **150**, 1093–1104.

Ehneß R, Roitsch T. 1997. Co-ordinated induction of mRNAs for extracellular invertase and a glucose transporter in *Chenopodium rubrum* by cytokinins. The Plant Journal **11**, 539–548.

Else MA, Coupland D, Dutton L, Jackson MB. 2001. Decreased root hydraulic conductivity reduces leaf water potential, initiates stomatal closure and slows leaf expansion in flooded plants of castor oil (*Ricinus communis*) despite diminished delivery of ABA from the roots to shoots in xylem sap. Physiologia Plantarum **111**, 46–54.

Fernandez J, Marroquin-Guzman M, Wilson RA. 2014. Mechanisms of nutrient acquisition and utilization during fungal infections of leaves. Annual Review of Phytopathoglogy **52**, 155–174.

Fernie AR, Bachem CW, Helariutta Y, *et al*. 2020. Synchronization of developmental, molecular and metabolic aspects of source–sink interactions. Nature Plants **6**, 55–66.

Fichtner F, Dissanayake IM, Lacombe B, Barbier F. 2020a. Sugar and nitrate sensing: a multi-billion-year story. Trends in Plant Science **26**, 352–374.

Fichtner F, Olas JJ, Feil R, Watanabe M, Krause U, Hoefgen R, Stitt M, Lunn JE. 2020b. Functional features of TREHALOSE-6-PHOSPHATE SYNTHASE1, an essential enzyme in Arabidopsis. The Plant Cell **32**, 1949–1972.

Fichtner F, Lunn JE. 2021. The role of trehalose 6-phosphate (Tre6P) in plant metabolism and development. Annual Review of Plant Biology **72**, 737–760.

Figueroa CM, Feil R, Ishihara H, *et al*. 2016. Trehalose 6–phosphate coordinates organic and amino acid metabolism with carbon availability. The Plant Journal **85**, 410–423.

Fukushima RS, Kerley MS. 2011. Use of lignin extracted from different plant sources as standards in the spectrophotometric acetyl bromide lignin method. Journal Agriculture Food Chemistry **59**, 3505–3509.

Gago J, Daloso DM, Figueroa CM, Flexas J, Fernie AR, Nikoloski Z. 2016. Relationships of leaf net photosynthesis, stomatal conductance, and mesophyll conductance to primary metabolism: a multispecies meta-analysis approach. Plant Physiology **171**, 265–279.

Giavalisco P, Li Y, Matthes A, *et al*. 2011. Elemental formula annotation of polar and lipophilic metabolites using ^{13}C, ^{15}N and ^{34}S isotope labelling, in combination with high-resolution mass spectrometry. The Plant Journal **68**, 364–376.

Gibson SI. 2005. Control of plant development and gene expression by sugar signaling. Current Opinion in Plant Biology **8**, 93–102.

Gohlke J, Deeken R. 2014. Plant responses to *Agrobacterium tumefaciens* and crown gall development. Frontiers in Plant Science **5**, 155.

Hane JK, Paxman J, Jones DAB, Oliver RP, de Wit P. 2020. "CATAStrophy," a genome-informed trophic classification of filamentous

plant pathogens – how many different types of filamentous plant pathogens are there? Frontiers in Microbiology **10**, 3088.

Hayes MA, Feechan A, Dry IB. 2010. Involvement of abscisic acid in the coordinated regulation of a stress-inducible hexose transporter (VvHT5) and a cell wall invertase in grapevine in response to biotrophic fungal infection. Plant Physiology **153**, 211–221.

Hedger JN, Pickering V, Aragundi J. 1987. Variability of populations of the witches' broom disease of cocoa (*Crinipellis perniciosa*). Transactions of the British Mycological Society **88**, 533–546.

Horbach R, Navarro-Quesada AR, Knogge W, Deising HB. 2011. When and how to kill a plant cell: infection strategies of plant pathogenic fungi. Jounal of Plant Physiology **168**, 51–62.

Horst RJ, Doehlemann G, Wahl R, Jofmann J, Schniedl A, Kahmann R, Kämper J, Voll LM. 2010. A model of *Ustilago maydis* leaf tumor metabolism. Plant Signaling and Behavior **5**, 1446–1449.

Huai B, Yang Q, Qian Y, Qian W, Kang Z, Liu J. 2019. ABA-induced sugar transporter TaSTP6 promotes wheat susceptibility to stripe rust. Plant Physiology **181**, 1328–1343.

Huai B, Yang Q, Wei X, Pan Q, Kang Z, Liu J. 2020. TaSTP13 contributes to wheat susceptibility to stripe rust possibly by increasing cytoplasmic hexose concentration. BMC Plant Biology **20**, 1–17.

Immanen J, Nieminen K, Smolander OP, *et al*. 2016. Cytokinin and auxin display distinct but interconnected distribution and signaling profiles to stimulate cambial activity. Current Biology **26**, 1990–1997.

Jensen WA. 1962. Botanical histochemistry: principles and practice. San Francisco: W.H. Freeman & Co.

Janusz G, Pawlik A, Sulej J, Świderska-Burek U, Jarosz-Wilkołazka A, Paszczyński A. 2017. Lignin degradation, microorganisms, enzymes involved, genomes analysis and evolution. FEMS Microbiology Reviews **41**, 941–962.

Kim SH, Lam PY, Lee MH, Jeon HS, Tobimatsu Y, Park OK. 2020. The Arabidopsis R2R3 MYB transcription factor MYB15 is a key regulator of lignin biosynthesis in effector-triggered immunity. Frontiers in Plant Science **11**, 1456.

Kolde R. 2018. pheatmap: Pretty heatmaps. R package v. 1.0.10. https://CRAN.R-project.org/package=pheatmap. Accessed February 2022.

Kuromori T, Seo M, Shinozaki K. 2018. ABA transport and plant water stress responses. Trends in Plant Science **23**, 513–522.

Lemoine R, La Camera S, Atanassova R, *et al*. 2013. Source-to-sink transport of sugar and regulation by environmental factors. Frontiers in Plant Science **4**, 272.

Li S, Li X, Wei Z, Liu F. 2020. ABA-mediated modulation of elevated CO_2 on stomatal response to drought. Current Opinion in Plant Biology **56**, 174–180.

Lindeberg G, Molin K. 1949. Notes on the physiology of the cacao parasite *Marasmius perniciosus*. Physiologia Plantarum **2**, 138–144.

Lisboa DO, Evans HC, Araújo JP, Elias SG, Barreto RW. 2020. *Moniliophthora perniciosa*, the mushroom causing witches' broom disease of cacao: insights into its taxonomy, ecology and host range in Brazil. Fungal Biology **124**, 983–1003.

Liu J, Moore S, Chen C, Lindsey K. 2017. Crosstalk complexities between auxin, cytokinin, and ethylene in *Arabidopsis* root development: from experiments to systems modeling, and back again. Molecular Plant **10**, 1480–1496.

Liu C, Yu H, Rao X, Li L, Dixon RA. 2021. Abscisic acid regulates secondary cell-wall formation and lignin deposition in *Arabidopsis thaliana* through phosphorylation of NST1. Proceedings of the National Academy of Sciences **118**, e2010911118.

Logan BA, Reblin JS, Zonana DM, *et al*. 2013. Impact of eastern dwarf mistletoe (*Arceuthobium pusillum*) on host white spruce (*Picea glauca*) development, growth and performance across multiple scales. Physiologia Plantarum **147**, 502–513.

Marelli JP, Maximova SN, Gramacho KP, Kang S, Guiltinan MJ, *et al*. 2009. Infection biology of *Moniliophthora perniciosa* on *Theobroma cacao* and alternate solanaceous hosts. Tropical Plant Biology **2**, 149–160.

Martínez-Bello L, Moritz T, López-Díaz I. 2015. Silencing C19-GA 2-oxidases induces parthenocarpic development and inhibits lateral branching in tomato plants. Journal of Experimental Botany **66**, 5897–5910.

Matei A, Ernst C, Günl M, Thiele B, Altmüller J, Walbot V, Usadel B, Doehlemann G. 2018. How to make a tumour: cell type specific dissection of *Ustilago maydis*-induced tumour development in maize leaves. New Phytologist **217**, 1681–1695.

Matías-Hernández L, Aguilar-Jaramillo AE, Cigliano RA, Sanseverino W, Pelaz S. 2016. Flowering and trichome development share hormonal and transcription factor regulation. Journal of Experimental Botany **67**, 1209–1219.

McIntyre KE, Bush DR, Argueso CT. 2021. Cytokinin regulation of source-sink relationships in plant-pathogen interactions. Frontiers in Plant Science **12**, 677585.

Michniewicz M, Ho CH, Enders TA, *et al*. 2019. TRANSPORTER OF IBA1 links auxin and cytokinin to influence root architecture. Developmental Cell **50**, 599–609.

Mondego JM, Carazzolle MF, Costa GG, *et al*. 2008. A genome survey of *Moniliophthora perniciosa* gives new insights into witches' broom disease of cacao. BMC Genomics **9**, 548.

Montero P, Vilar JA. 2014. TSclust: an R package for time series clustering. Journal of Statistical Software **62**, 1–43.

Morrison EN, Emery RJN, Saville BJ. 2017. Fungal derived cytokinins are necessary for normal *Ustilago maydis* infection of maize. Plant Pathology **66**, 726–742.

Muller B, Guédon Y, Passot S, Lobet G, Nacry P, Pagès L, Wissuwa M, Draye X. 2019. Lateral roots: random diversity in adversity. Trends in Plant Science **24**, 810–825.

Nardini A, Tyree MT. 1999. Root and shoot hydraulic conductance of seven *Quercus* species. Annals of Forest Science **56**, 371–377.

Orchard JE, Hardwick K. 1988. Photosynthesis, carbohydrate translocation and metabolism of host and fungal tissues in cacao seedlings infected with *Crinipellis perniciosa*. In: 10th International Cocoa Research Conference. Santo Domingo, Dominican Republic, 17–23 May 1987. Proceedings. Lagos: Cocoa Producers Alliance, 325–330.

Osono T. 2020. Functional diversity of ligninolytic fungi associated with leaf litter decomposition. Ecological Research **35**, 30–43.

Patro R, Duggal G, Love MI, Irizarry RA, Kingsford C. 2017. Salmon provides fast and bias-aware quantification of transcript expression. Nature Methods **14**, 417–419.

Pertry I, Václavíková K, Depuydt S, *et al*. 2009. Identification of *Rhodococcus fascians* cytokinins and their modus operandi to reshape the plant. Proceedings of the National Academy of Sciences USA **106**, 929–934.

Pierre S, Griffith GW, Morphew RM, Mur LAJ, Scott IM. 2017. Saprotrophic proteomes of biotypes of the witches' broom pathogen *Moniliophthora perniciosa*. Fungal Biology **121**, 743–753.

Pino LE, Lombardi-Crestana S, Azevedo MS, Scotton DC, Borgo L, Quecini V, Figueira A, Peres LEP. 2010. The *Rg1* allele as a valuable tool for genetic transformation of the tomato 'Micro-Tom' model system. Plant Methods **6**, 23.

Pivovaroff AL, Sack L, Santiago LS. 2014. Coordination of stem and leaf hydraulic conductance in southern California shrubs, a test of the hydraulic segmentation hypothesis. New Phytologist **203**, 842–850.

Pommerrenig B, Müdsam C, Kischka D, Neuhaus HE. 2020. Treat and trick: common regulation and manipulation of sugar transporters during sink establishment by the plant and the pathogen. Journal of Experimental Botany **71**, 3930–3940.

Proels RK, Roitsch T. 2009. Extracellular invertase LIN6 of tomato, a pivotal enzyme for integration of metabolic, hormonal, and stress signals is regulated by a diurnal rhythm. Journal of Experimental Botany **60**, 1555–1567.

Purdy LH, Schmidt RA. 1996. Status of cacao witches' broom: Biology, epidemiology, and management. Annual Review of Phytopathology **34**, 573–594.

R Core Team. 2020. R: a language and environment for statistical computing. Vienna, Austria: R Foundation for Statistical Computing. https://www.R-project.org/.

Ramachandran P, Augstein F, Mazumdar S, Nguyen TV, Minima EA, Melnyk CW, Carlsbecker A. 2021. Abscisic acid signaling activates distinct VND transcription factors to promote xylem differentiation in *Arabidopsis*. Current Biology **31**, 1–9.

Roessner U, Wagner C, Kopka J, Trethewey RN, Willmitzer L. 2000. Simultaneous analysis of metabolites in potato tuber by gas chromatography–mass spectrometry. The Plant Journal **23**, 131–142.

Rojas CM, Senthil-Kumar M, Tzin V, Mysore KS. 2014. Regulation of primary plant metabolism during plant-pathogen interactions and its contribution to plant defense. Frontiers in Plant Science **5**, 17.

Roman H, Girault T, Barbier F, *et al*. 2016. Cytokinins are initial targets of light in the control of bud outgrowth. Plant Physiology **172**, 489–509.

Rouhi V, Samson R, Lemeur R, Van Damme P. 2007. Photosynthetic gas exchange characteristics in three different almond species during drought stress and subsequent recovery. Environmental and Experimental Botany **59**, 117–129.

Rudgard SA. 1986. Witches' broom disease of cocoa in Rondonia, Brazil: Pod losses. International Journal of Pest Management **32**, 24–26.

Sakr S, Wang M, Dédaldéchamp F, Perez-Garcia MD, Ogé L, Hamama L, Atanassova R. 2018. The sugar-signaling hub: overview of regulators and interaction with the hormonal and metabolic network. International Journal of Molecular Sciences **19**, 2506.

Scarpari LM, Meinhardt LW, Mazzafera P, Pomella AWV, Schiavinato MA, Cascardo JCM, Pereira GAG. 2005. Biochemical changes during the development of witches' broom, the most important disease of cocoa in Brazil caused by *Crinipellis perniciosa*. Journal of Experimental Botany **56**, 865–877.

Schultz JC, Appel HM, Ferrieri A, Arnold TM. 2013. Flexible resource allocation during plant defense responses. Frontiers in Plant Science **4**, 324.

Sena K, Alemanno L, Gramacho KP. 2014. The infection process of *Moniliophthora perniciosa* in cacao. Plant Pathology **63**, 1272–1281.

Smith GR, Finlay RD, Stenlid J, Vasaitis R, Menkis A. 2017. Growing evidence for facultative biotrophy in saprotrophic fungi, data from microcosm tests with 201 species of wood-decay basidiomycetes. New Phytologist **215**, 747–755.

Soneson C, Love MI, Robinson MD. 2015. Differential analyses for RNA-seq, transcript-level estimates improve gene-level inferences. F1000Research **4**, 1521.

Sosso D, Van Der Linde K, Bezrutczyk M, Schuler D, Schneider K, Kämper J, Walbot V. 2019. Sugar partitioning between *Ustilago maydis* and its host *Zea mays* L during infection. Plant Physiology **179**, 1373–1385.

Stacklies W, Redestig H, Scholz M, Walther D, Selbig J. 2007. pcaMethods—a bioconductor package providing PCA methods for incomplete data. Bioinformatics **23**, 1164–1167.

Sweetlove LJ, Beard KF, Nunes-Nesi A, Fernie AR, Ratcliffe RG. 2010. Not just a circle: flux modes in the plant TCA cycle. Trends in Plant Science **15**, 462–470.

Tauzin AS, Giardina T. 2014. Sucrose and invertases: a part of the plant defense response to the biotic stresses. Frontiers in Plant Science **5**, 293.

Tegeder M, Masclaux-Daubresse C. 2018. Source and sink mechanisms of nitrogen transport and use. New Phytologist **217**, 35–53.

Teixeira PJPL, Thomazella DPDT, Reis O, *et al*. 2014. High-resolution transcript profiling of the atypical biotrophic interaction between *Theobroma cacao* and the fungal pathogen *Moniliophthora perniciosa*. The Plant Cell **26**, 4245–4269.

Thimm O, Bläsing O, Gibon Y, *et al*. 2004. MAPMAN: a user-driven tool to display genomics data sets onto diagrams of metabolic pathways and other biological processes. The Plant Journal **37**, 914–939.

Tyagi K, Maoz I, Kochanek B, Sela N, Lerno L, Ebeler SE, Lichter A. 2021. Cytokinin but not gibberellin application had major impact on the phenylpropanoid pathway in grape. Horticulture Research **8**, 51.

Veillet F, Gaillard C, Coutos-Thévenot P, La Camera S. 2016. Targeting the *AtCWIN1* gene to explore the role of invertases in sucrose transport in roots and during *Botrytis cinerea* infection. Frontiers in Plant Science **7**, 1899.

Veillet F, Gaillard C, Lemonnier P, Coutos-Thévenot P, La Camera S. The molecular dialogue between *Arabidopsis thaliana* and the necrotrophic fungus *Botrytis cinerea* leads to major changes in host carbon metabolism. Scientific Reports **7**, 17121.

Walerowski P, Gündel A, Yahaya N, Truman W, Sobczak M, Olszak M, Rolfe S, Borisjuk L, Malinowski R. 2018. Clubroot disease stimulates early steps of phloem differentiation and recruits SWEET sucrose transporters within developing galls. The Plant Cell **30**, 3058–3073.

Walters DR, McRoberts N. 2006. Plants and biotrophs: a pivotal role for cytokinins? Trends in Plant Science **11**, 581–586.

Werner T, Motyka V, Laucou V, Smets R, Van Onckelen H, Schmülling T, *et al*. 2003. Cytokinin-deficient transgenic Arabidopsis plants show multiple developmental alterations indicating opposite functions of cytokinins in the regulation of shoot and root meristem activity. The Plant Cell **15**, 2532–2550.

Xiong D, Nadal M. 2020. Linking water relations and hydraulics with photosynthesis. The Plant Journal **101**, 800–815.

Zhang W, Wang S, Yu F, Tang J, Yu L, Wang H, Li J. 2019a. Genome-wide identification and expression profiling of sugar transporter protein (STP) family genes in cabbage (*Brassica oleracea var. capitata L.*) reveals their involvement in clubroot disease responses. Genes **10**, 71.

Zhang W, Wang S, Yu F, Tang J, Shan X, Bao K, Yu L, Wang H, Fei Z, Li J. 2019b. Genome-wide characterization and expression profiling of *SWEET* genes in cabbage (*Brassica oleracea* var. *capitata* L.) reveal their roles in chilling and clubroot disease responses. BMC Genomics **20**, 93.

Zhao C, Avci U, Grant EH, Haigler CH, Beers EP. 2008. XND1, a member of the NAC domain family in *Arabidopsis thaliana*, negatively regulates lignocellulose synthesis and programmed cell death in xylem. The Plant Journal **53**, 425–436.

Zell MB, Fahnenstich H, Maier A, *et al*. 2010. Analysis of Arabidopsis with highly reduced levels of malate and fumarate sheds light on the role of these organic acids as storage carbon molecules. Plant Physiology **152**, 1251–1262.

Zhong R, Richardson EA, Ye ZH. 2007. The MYB46 transcription factor is a direct target of SND1 and regulates secondary wall biosynthesis in *Arabidopsis*. The Plant Cell **19**, 2776–2792.

Zhong R, Ye ZH. 2012. MYB46 and MYB83 bind to the SMRE sites and directly activate a suite of transcription factors and secondary wall biosynthetic genes. Plant and Cell Physiology **53**, 368–380.